

ALBERT-LUDWIGS UNIVERSITÄT FREIBURG

Bachelorthesis

JUPYTER NOTEBOOK:
A proof-of-principle notebook using
ATLAS dijet data

Submitted for the Degree of
Bachelor of Science in Physics

by

Leonie Hermann



Supervision: Prof. Markus Schumacher

Faculty of Mathematics and Physics
University of Freiburg, Germany

Erklärung

Hiermit versichere ich, die eingereichte Bachelorarbeit selbständig verfasst und keine anderen als die von mir angegebenen Quellen und Hilfsmittel benutzt zu haben. Wörtlich oder inhaltlich verwendete Quellen wurden entsprechend den anerkannten Regeln wissenschaftlichen Arbeitens (lege artis) zitiert. Ich erkläre weiterhin, dass die vorliegende Arbeit noch nicht anderweitig als Bachelorarbeit eingereicht wurde.

Ort, Datum

Unterschrift

Abstract

This is an elaboration and explanation of the Jupyter notebook “*A proof-of-principle notebook using dijet events*” and explains the features and the theory behind the search beyond the Standard Model by investigating dijet events. In the Jupyter notebook different techniques to compare data with the background prediction are applied. The comparison of bin-by-bin methods showed, that calculating and the depicting the significance of a Poisson distribution gives the most reliable results.

The dijet events of a data set recorded in 2015 and 2016 with the ATLAS detector in proton-proton collisions at $\sqrt{s} = 13$ TeV corresponding to an integrated luminosity of 37 fb^{-1} were investigated. The dijet data set did not show any significant deviation from the background-only hypothesis. The significance of all bins is below 2.4 standard deviations.

Furthermore, the BumpHunter and the TailHunter hypothesis hyper test are introduced. The implemented hypothesis hyper test BumpHunter algorithm came the same conclusions as found by the official search paper with the most significant bump at $m_{jj} = 4.2825 - 4.5495$ TeV with a p -value ≈ 0.69 . The window has no significant deviations. The TailHunter evaluated the most significant tail at $m_{jj} = 7.904 - 8.364$ TeV with p -value ≈ 0.24 . This corresponds to 0.7 standard deviations. Thus, the results from the ATLAS experiment can be reproduced and presented in an easier way.

Zusammenfassung

Dies ist die Ausarbeitung zum Jupyter Notebook mit dem Namen „*A proof-of-principle notebook using dijet events*“. Es werden die Theorie, das Experiment und die Komponenten im Notebook erklärt. Das Notebook zeigt verschiedene Möglichkeiten auf, wie ein Datensatz mit einer Vorhersage verglichen werden kann. Beim „Bin-für-Bin“-Vergleich gilt als verlässlichste Methode das Berechnen der Signifikanz einer Poisson-Verteilung. Dabei wurden die 2-Jets Ereignisse untersucht, die aus einem Datensatz stammen, der in den Jahren 2015 und 2016 mit einer integrierten Luminosität von 37 fb^{-1} von dem ATLAS Detektor bei einer Schwerpunktsenergie von $\sqrt{s} = 13$ TeV in Proton-Proton Kollisionen aufgenommen wurde. In dem untersuchten Datensatz wurden keine signifikanten Abweichungen gefunden. Für alle Bins liegt das Ergebnis unter 2.4 Standardabweichungen. Daneben wurden auch der *BumpHunter* und der *TailHunter* Hypothesentest eingeführt. Der *BumpHunter* hat den signifikantesten Überschuss im Bereich $m_{jj} = 4.2825-4.5495$ TeV gefunden, wobei der p -value ≈ 0.69 sehr groß ist und daher der Überschuss nicht signifikant ist. Der *TailHunter* hat festgestellt, dass $m_{jj} = 7.904 - 8.364$ TeV mit p -value ≈ 0.24 der am meisten signifikante *Tail*-Abschnitt ist. Die Abweichung entspricht allerdings nur 0.7 Standardabweichungen. Beim Vergleich mit den offiziellen Ergebnissen der ATLAS-Kollaboration hat sich gezeigt, dass die Ergebnisse reproduzierbar sind und auch in einfacherer Weise dargestellt werden können.

Contents

1	Introduction	3
2	Theory	4
2.1	The Standard Model	4
2.1.1	Particles	5
2.1.2	Interactions	5
2.1.3	Higgs boson	6
2.2	Jet production	6
2.3	New physics beyond the Standard Model	8
2.4	Search for a new resonance	10
3	The Experiment	11
3.1	The Large Hadron Collider	11
3.2	The ATLAS detector	12
3.2.1	Coordinate System	12
3.2.2	Detector Components	13
4	Programming Tools	17
4.1	Project Jupyter and Jupyter notebooks	17
4.1.1	Installation	17
4.2	The Proof-of-Principle notebook using dijet events	18
4.2.1	Usage	19
5	Selection and Background Estimation	24
5.1	Reconstruction of Jets	24
5.2	Calibration of Jets	25
5.3	Selection criteria	27
5.4	Background estimation	28
6	Basic Principles of Statistics	32
6.1	Probability models for counting experiments	32
6.2	Statistical Hypothesis Testing	33
6.2.1	General operation of a hypothesis test	33
6.2.2	Bin-by-bin hypothesis testing	35
6.2.3	Hypothesis hyper test	36
7	Statistical Analysis and Implementation	37
7.1	Bin-by-Bin Techniques	38
7.1.1	Absolute and Relative Difference	38
7.1.2	Gaussian approximation of the significance	40
7.1.3	The Significance	43
7.2	Comparison of the Bin-by-Bin Analyze	45
7.3	BumpHunter and TailHunter algorithm as a global comparison technique	46
7.3.1	The Bumphunter algorithm	47
7.3.2	Generalization of the BumpHunter: TailHunter	50
7.4	Proof-of-Principle: Sanity Check	53
8	Conclusion	55

A Statistics	56
A.1 Derivation of Poisson distribution	56
A.1.1 Approximation of Binomial to Poisson distribution	56
A.1.2 Derivation with Poisson assumptions	57
A.2 Approximation of Poisson to Gaussian distribution	58
Bibliography	59

1 Introduction

In order to understand how matter is built up and how it interacts, physicists create theories which describe and explain phenomena. Looking at the smallest discovered particles, called elementary particles, models to explain are introduced. Nearly all experimental observations in particle physics are described by the Standard Model. However, the Standard Model cannot describe all phenomena such as dark matter and dark energy. Therefore, physicists search for expansions and new possible theories. While theorists try to calculate the behaviour of particles, experimental physicists design and run big experiments like the ATLAS experiment at the Large Hadron Collider at CERN [1]. There, particles created in proton-proton collisions are recorded by the ATLAS detector [2].

The analysis of the recorded data takes a long procedure, from reconstruction, calibration to the event selection over the statistical analysis [3] to the final results. For early university students and pupils in school the analysis appeared to be too complicated to be understandable. In order to further introduce students to particle physics, statistical methods and analysis procedures are explained at an appropriate level. This thesis consists of a written elaboration on these subjects and a detailed Jupyter notebook.

The basis of the project is the Jupyter notebook called “*A proof-of-principle notebook using dijet events*” in which the analysis is explained step-wise. A Jupyter notebook [4] is an interactive programming tool which is run in the programming language Python and where explanations, graphics and code are combined. Python is chosen as the language is comparatively easy for novice programmers to learn and to understand. Jupyter notebooks are used, because Jupyter is an open-source program which can be run online or offline and is accessible for everyone for free. The written elaboration complements the Jupyter notebook especially with regards to the theory, experiments and statistical methods. While the notebook is kept compact, the written report explains the features in more detail.

Exemplary, one data set [3] is used which was already analyzed by the ATLAS Collaboration. The data set includes dijet events recorded in 2015 and 2016 with the ATLAS detector in proton-proton collisions at $\sqrt{s} = 13$ TeV corresponding to an integrated luminosity of 37 fb^{-1} . Dijet events are predicted in processes of Quantum Chromo Dynamic and described by the Standard Model in a smoothly decreasing function for higher invariant dijet masses m_{jj} . However, in other models beyond the Standard Model, dijet events could be created by the decay of a new particle. This would create an excess of data in the invariant dijet mass m_{jj} spectrum. The mass of the new particle is equal to m_{jj} where the excess in the m_{jj} distribution is found.

Here, the statistical analysis becomes important. The Jupyter notebook explains, how data can be compared with a background prediction and how the result can be interpreted. First, the data and the background prediction are compared bin-by-bin [5]. Different ways of depicting the differences are shown and discussed as the absolute and the relative difference, an approximation of the significance and the actual significance. Secondly, a global technique for investigating the differences between data and background prediction is applied. Two hypothesis hyper tests are implemented: The BumpHunter and the TailHunter algorithm [6]. The BumpHunter investigates several ranges in the spectrum and points out the most significant excess. The TailHunter is a generalization of the BumpHunter looking for the most significant tail. The results are then compared with the official result of the ATLAS collaboration.

2 Theory

This chapter introduces the Standard Model (SM) [7, 8, 9] of particle physics, which describes almost all experimental observations in particle physics. The properties of the elementary particles and their interactions are described. This chapter is based on Ref. [10, 11, 12, 13].

The second part explains the jet production based on Ref. [14, 15, 16] and focuses on jets produced by hard scattering in Quantum Chromo Dynamics processes. As a motivation for the search, models beyond the Standard Model are presented based on Ref. [16, 17, 18]. The idea of the dijet analysis is then given in Section 2.4 [3].

2.1 The Standard Model

The SM was introduced in the late 1960's and describes the elementary particles and their interactions through three of four fundamental forces: electromagnetic, weak and strong force. The fourth force, the gravitational force, is not included in the SM. Elementary particles are quantum objects without permanent substructure. An overview of the particle content in the SM is given in Fig. 2.1. Depending on the characteristics of the elementary particle, it is classified into two classes by the SM. Elementary particles which build up the matter have a half-integer spin, an anti-symmetric wave function and belong to the class called fermions. There are three generations of fermions with increasing mass. Interactions are described by the exchange of vector bosons with integer spin of 1. One scalar boson with spin zero is the Higgs boson.

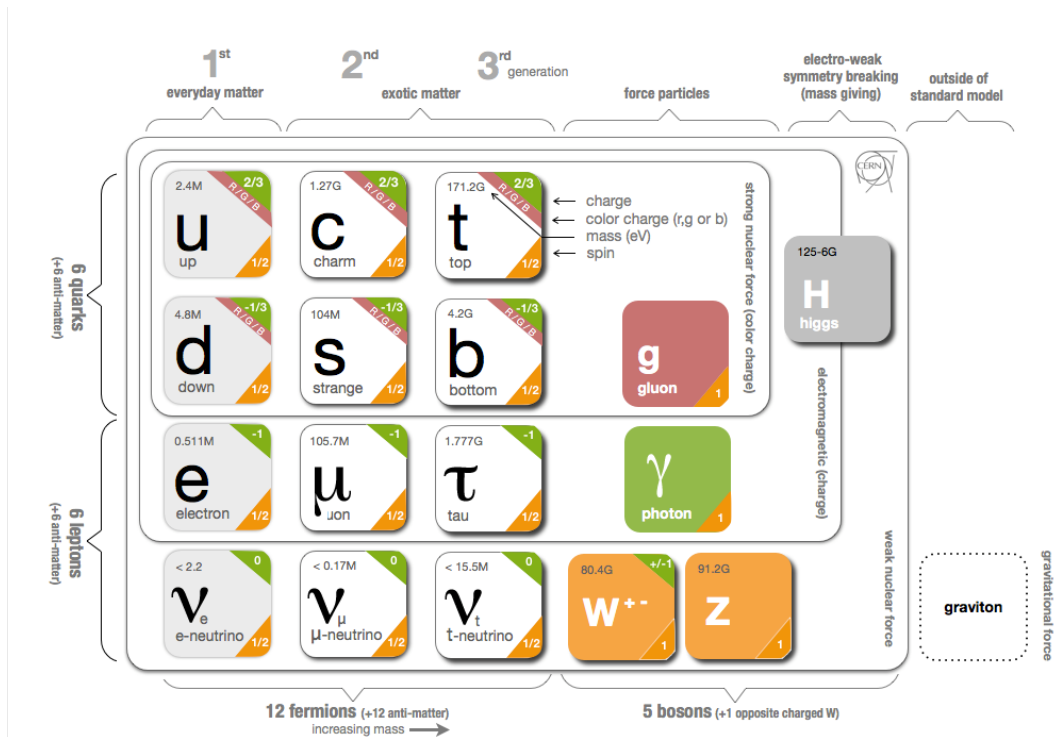


Figure 2.1: The particles of the Standard Model in particle physics [19].

2.1.1 Particles

Fermions are particles with spin $s = 1/2$ and are divided into quarks and leptons. Each particle has an antiparticle with the same mass $\bar{m} = m$, the opposite electric charge $\bar{Q} = -Q$ and the opposite magnetic moment $\bar{\mu} = -\mu$. All additional quantum numbers are inverted eg. colors.

As shown on the left hand side in Fig. 2.1, 6 quarks (+ 6 anti quarks) and 6 leptons (+ anti leptons) make up to 24 fermions in total.

Quarks The quark family consists of six distinct quark types which occur in pairs in three generations. The first generation of quarks consist of the up-quark u and the down-quark d , the second generation of the charm-quark c and the strange-quark s , and the third generation of the top-quark t and the bottom-quark b . Up-, charm- and top-quark are charged with $Q = +2/3 e$ and down-, strange- and bottom-quark with $Q = -1/3 e$. Beside the electric charge, quarks carry also a color charge of either red, green, blue or an anti-color anti-red, anti-green, anti-blue. Quarks cannot be isolated due to the color confinement. Only combinations with a total color of white can form stable matter. Such particles are called hadrons and are held together by the strong force. The constituents of a hadron are called partons. Three quarks with three different color charges like a proton p (uud) are called baryons. The combination of quark and anti-quark with color and anti-color like a pion π^+ ($u\bar{d}$) are called mesons. Those two possibilities are most common for producing a white colored particle. Quarks can interact with all force particles described in Section 2.1.2.

Leptons The three generations of leptonic particles are electron, muon and tau. The first generation is formed by the electron e^- and the electron-neutrino ν_e and their antiparticles, respectively. The muon μ^- , the muon-neutrino ν_μ and their antiparticles are the muonic leptons, and the last and heaviest generation is composed of the tau τ^- , the tau-neutrino ν_τ and their antiparticles. Neutrino antiparticles are marked with a bar on top, $\bar{\nu}$. The electron, muon and tau leptons are charged with $Q = -1 e$. This is illustrated by the minus sign⁻. By definition, their antiparticles are positively charged with $Q = +1 e$. Neutrinos are not charged ($Q = 0$) and almost massless. Leptons have no color charge and therefore they do not interact strongly. However, charged leptons interact electromagnetically and all leptons interact weakly.

A quantum number called lepton number L is defined by the type of lepton generation. In a elementary particle reaction this quantum number must be conserved. Each lepton generation has its own lepton number L_x which becomes $L_x = 1$ for leptons and $L_x = -1$ for anti leptons with $x = e, \mu$ or τ .

2.1.2 Interactions

Vector bosons are interaction particles with spin $s = 1$ and symmetric wave functions. The photon γ responsible for electromagnetic interaction, the W^\pm - and Z -boson for weak interaction and the gluon g for strong interaction are in the class of vector bosons.

The three interaction types in the SM are summarized in Table 2.1. Each interaction type is defined by its characteristic charge. The charge is a fundamental property of a particle. It can only change by interaction with the interaction particle, respectively. Charge is quantised and conserved in a system. The charge of the whole system is given by the sum of all particles in the system with this specific charge.

Table 2.1: The characteristics of three of the four fundamental forces [12].

	Weak force	Electromagnetic force	Strong force
Mediator	weak vector bosons (W^+, W^-, Z^0)	photon (γ)	gluon (g)
Mass of the mediator	$W^\pm \sim 80.4 \text{ GeV}$ [19] $Z^0 \sim 91.2 \text{ GeV}$ [19]	0	0
Range	$\sim 10^{-18} \text{ m}$	∞	$\sim 10^{-15} \text{ m}$
Fermions affected	all	electrically charged	color charged
Relative strength to the strong force	$\sim 10^{-38}$	$\sim 10^{-2}$	1

The three forces are described by three theories: Quantum Electro Dynamics (QED)[20, 21, 22], Quantum Flavor Dynamics (QFD) [7, 8, 9] and Quantum Chromo Dynamics (QCD) [23, 24].

QED is the theory of electromagnetic interaction between the photon γ and electric charged particles. The photon has no mass and no electric charge. The electromagnetic force ranges infinitely and compared to the other two interactions, it is the second strongest one.

The theory of weak interaction is QFD. The charge of QFD is called weak-isospin and is for all fermions $I_W = 1/2$, for the W^- and Z -bosons $I_W = 1$ and for the photon γ and the gluon g $I_W = 0$. The three different mediators are W^- , W^+ and Z^0 bosons. Those are the only bosons that acts on all fermions. The weak force is weak at low energies due to the comparable high mass of the bosons.

QCD is the theory of strong interaction between quarks and the force carrier is the gluon. QCD defines color charge as fundamental property for strong interaction and is characterized by the color charges. The massless gluon carries a color and an anti-color charge and therefore it couples to color charge. Combining different colors and anti-colors in the gluon result in eight different types of gluons, also called color octet. By interaction of gluons with quarks, the quarks change their color charge. QCD can explain color confinement described earlier.

2.1.3 Higgs boson

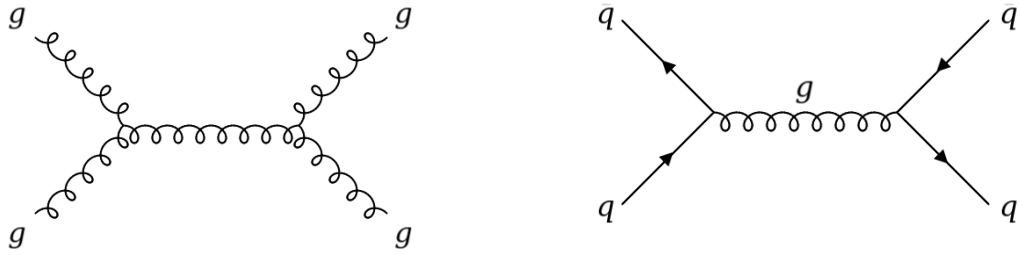
The Higgs boson has been discovered in 2012 [25] and the associated Brout-Englert-Higgs mechanism is responsible for the mass of fermions and bosons. The Higgs boson has spin zero, no charge and no color charge. Its mass is $m_H = 125.09 \text{ GeV}$ [19]. In the Higgs mechanism [26, 27], the Higgs boson originates from the so-called Higgs field which fills up the whole space. By interaction of a particle with it, the particle acquires mass. The mass is proportional to the coupling strength between the field and the particle.

2.2 Jet production

Hadronization is the process when gluons and quarks form colorless hadronic particles which move in the origin direction. A collimated flow of color-neutral particles moving, essentially, the same direction is called a jet. The reconstruction of jet gives properties about the initial particle. Jets are produced in high energy collisions of hadrons like in a proton-proton (pp) collider at the LHC.

Taking here a pp-collision as example: Protons consists of quarks and gluons. These constituents are called partons. In a collision at high energies, the colliding partons transfer a large part of their momentum between each other in the interaction. This is typical for a hard scattering process.

Jets can be produced by standard QCD processes such as gluon-gluon scattering and quark-antiquark annihilation. In both cases, a pair of partons can be created. Corresponding Feynman diagrams at leading order are shown in Fig. 2.2. Next-to-leading order processes also contribute to the di-parton production. Then, additional partons are emitted or virtual loops are included.



(a) Gluon-gluon scattering producing a pair of gluons ($gg \rightarrow gg$). (b) Quark anti-quark annihilation producing quark and anti-quark ($q\bar{q} \rightarrow q\bar{q}$).

Figure 2.2: Feynman diagrams of partonic processes producing parton pairs and causing jets. Figures adapted from Ref. [28].

The partons produced in those processes can create more partons at high energies as the reactions $g \rightarrow gg$ or $g \rightarrow q\bar{q}$. So-called parton showers are produced at small angles. In this collimated flow of partons, the effect of hadronization dominates at small energies. Due to color confinement, hadrons are built from partons. The hadrons move in the same direction as the partons with the same total energy in the form of jets.

Furthermore, new particles can be created by the interaction of partons. A Feynman diagram of this reaction is shown in Fig. 2.3. The decay of the particle X into a pair of partons can also cause hadronic showers. The particles in the shower have together the same four momenta like the resonance particle. They moving in the essentially the same direction, in a jet. Such a resonance particle could be the Z -boson for example or a new particle beyond the SM as explained in Section 2.3.

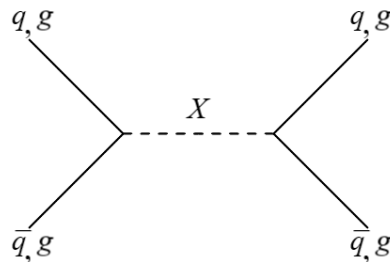


Figure 2.3: Feynman diagram of partons (q, \bar{q}, g) producing a particle X decaying into a pair of partons.

2.3 New physics beyond the Standard Model

Our universe consists to 4% of baryonic matter, 23% Dark Matter (DM) and the largest portions makes dark energy with about 73% [17]. The atomic part is well-described by the SM (cf. Section 2.1) however the SM does not have any explanations for the other parts. This is one empirical problem of the SM.

This section focuses on DM. Since the SM incorporates only the visible matter and its interactions, it cannot explain all experimentally observed phenomena. Especially in astrophysical measurements, there is evidence, that around 90% of the mass in a galaxy is DM. The important result of the properties of rotational curves is depicted in the following paragraph.

DM is postulated by different astrophysical observations: the properties of rotational curves, gravitational lensing, and hot gas in clusters. The idea of dark energy comes from observations of distant supernovae which are dimmer than the theory predicts [17]. The following part is based on Ref. [17].

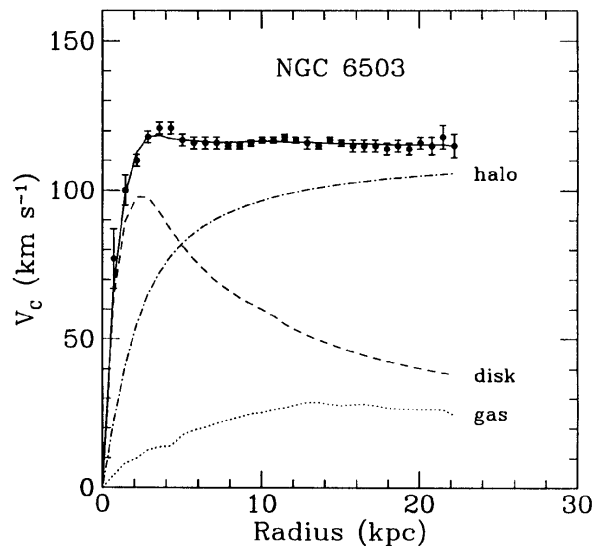


Figure 2.4: The rotational curve of a galaxy [29]. The halo curve shows the dark matter contribution for matching the data with the disk and gas curve.

Another indication of the existence of DM came by Ford and Rubin in the 1970s [30]. They calculated the velocity of objects in a galaxy according to Keplers laws and compared it to the experimental observations. Keplers laws predict an increase of the velocity by a rising distance to the galactic center. However, the measurements yield the velocity to be constant for large radii. This is presented in Fig. 2.4. Here, the velocity profile of the galaxy NGC 6503 is analyzed. The velocity is plotted as a function of the radius. The curve becomes flat which cannot be explained by adding up the visible matter from the disk and gas curve. The disk and gas curves in the figure represent the baryonic matter in the galaxy. The fact, that the measured velocity is flat, gives an indication that the galaxies are much heavier than assumed by the visible stellar objects. By introducing DM and calculating its velocity profile (halo), experimental observations can be explained. However, dark matter has not yet been detected. Theorists postulate models beyond the SM to explain dark matter and its behaviour. Some of those are used in the analysis as 'benchmark models' to set limits. A new mediator particle between the particles in the

SM and DM could be created causing the resonance.

The BSM benchmark theories considered in the dijet search are listed below. Not all of them are necessarily DM mediators.

- **W' , Z' and excited W^* boson:** W' and Z' are hypothetical gauge bosons heavier than their respective particle in the SM. The W' is described in the Sequential Standard model [31] and has the same charge, spin and couplings as the W^\pm bosons in the SM.

The Z' boson [32] is a possible dark matter mediator and also couples to quarks as shown in Fig. 2.5.

Another possible particle is the excited W^* boson which could solve the hierarchy problem that is further described in Ref. [33].

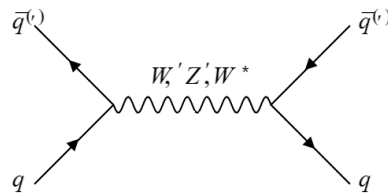


Figure 2.5: The bosons W' , Z' and W^* are produced by partons and decay into a pair of partons. Figure adapted from Ref. [34].

- **Excited quarks q^* :** In composite quark models [35] excited quarks are quarks with added energy and therefore they have a higher mass. The theory says that an excited quark contains other particles in it, which carry the higher energy. This leads to a not point-like shape of an excited quark. If the excited quark q^* decays into a pair of partons as shown in Fig. 2.6, a dijet m_{jj} resonance state would be created. By emitting for example a photon or a gluon, the excited quark could become the “normal” quark.

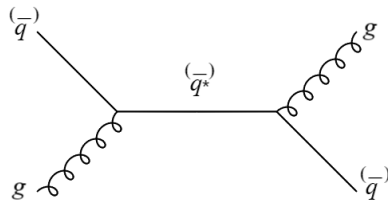


Figure 2.6: In the theory, the excited quark could be produced by the interaction of partons (gluons, quarks) and decay in a pair of partons causing dijet production. Figure adapted from Ref. [34].

- **Quantum black holes (qbh):** The gravitational force is not part of the SM model and much weaker than the other three fundamental forces. A qbh is a tiny self-gravitating black hole and part of the black hole model [36]. The theory of qbh [37] predicts so-called Hawking radiation that are spontaneously emitted particles by the black hole.

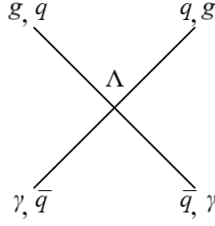


Figure 2.7: Possible interaction of partons with a quantum black hole Λ decaying into a 2-body final state. Figure adapted from Ref. [34].

2.4 Search for a new resonance

Theories beyond the SM predict new particles. New particles which couples to the SM can be searched for with the ATLAS detector. If a new resonant particle is produced by a pp -collision it can decay to two partons resulting in a dijet final state as described in Section 2.2. With the ATLAS detector, those events are measured so that the four momenta of the jets can be determined. Selecting dijet events with the jets back-to-back in the transverse plane, in nearly opposite directions (momentum conservation), the invariant dijet mass m_{jj} of the new particle can be calculated. Using the calibrated four momenta of both jets with the energy E_1 and the momentum \vec{p}_1 of the leading jet and the energy E_2 and the momentum \vec{p}_2 of the sub-leading jet, the invariant dijet mass m_{jj} is calculated by

$$m_{jj} = \sqrt{(E_1 + E_2)^2 - (\vec{p}_1 + \vec{p}_2)^2}. \quad (2.1)$$

A smooth, monotonically decreasing distribution of the dijet invariant mass m_{jj} is predicted for high m_{jj} ($\approx 1 - 8$ TeV) by QCD processes. Therefore, a new resonant state would be visible by an excess in the m_{jj} distribution.

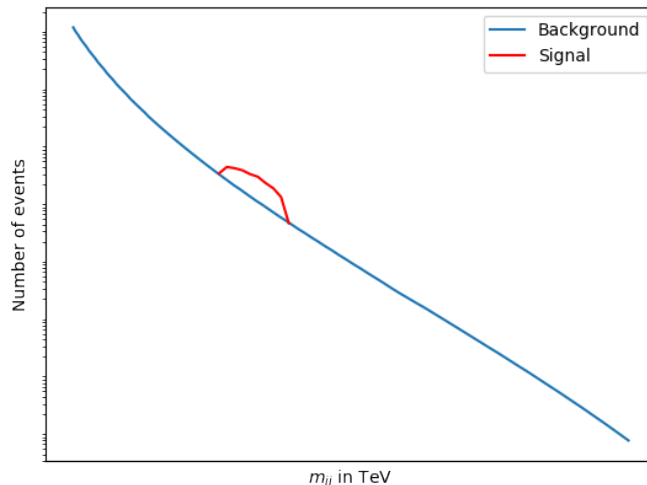


Figure 2.8: A sketch of showing the number of events against the invariant dijet mass m_{jj} is shown. The blue background function is smooth and decreasing with higher m_{jj} . A signal like in red plotted could occur in the distribution if a new particle is observed. Figure adapted from Ref. [38].

3 The Experiment

The data analyzed in this project have been collected in proton-proton collisions provided by the Large Hadron Collider (LHC [39]) and recorded with the ATLAS detector (A Toroidal LHC ApparatuS [40]). Both, the accelerator and the detector are part of the largest particle physics laboratory in the world - the European Organization for Nuclear Research (CERN) [1] and are introduced in this chapter based on Ref. [39, 40, 41].

3.1 The Large Hadron Collider

The LHC is currently the largest and most powerful man-made particle accelerator in the world. It is located at the border of France and Switzerland near Geneva in Switzerland and is part of CERN.

The LHC is a 27.6 km long circular accelerator placed in an underground tunnel which is 100–150 m below ground level. After the electron-positron e^-e^+ -collider LEP had been shut down in 2000, the LHC had its first run in 2008. It accelerates protons up to an energy of 7 TeV so that the maximum center of mass energy at collisions is 14 TeV. At the moment it runs at a center of mass energy of 13 TeV. Inside of two separate beam pipes, high energy proton bunches with a speed near the speed of light, travel clockwise or anticlockwise. In each of the 2808 bunches per beam, 1.2×10^{11} protons are accelerated, bend and focused by superconducting electromagnets. With a crossing rate of 40 MHz, the accelerator reaches 10^9 collisions per second [42].

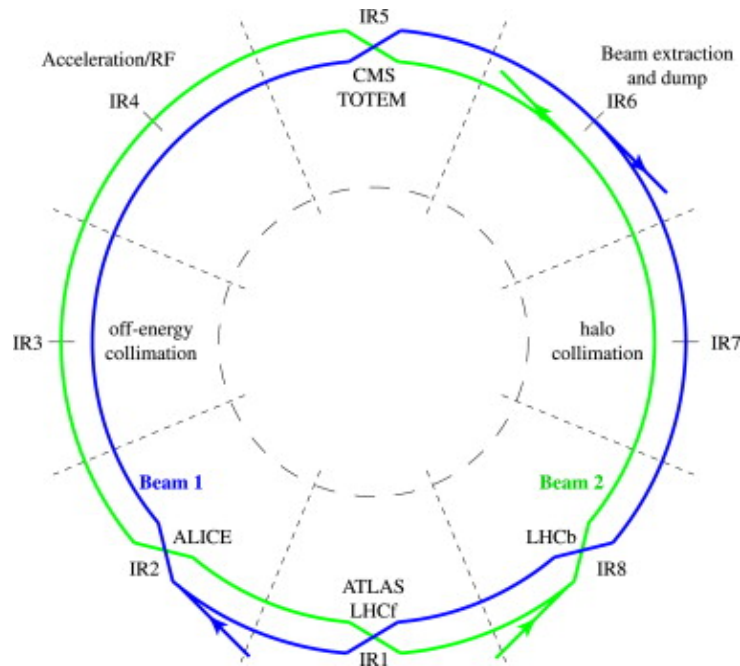


Figure 3.1: The figure shows the LHC complex [39] with the clockwise blue beam and the anticlockwise green beam. The positions of the experiments placed at the beam can be seen.

The LHC has four collision points as stated in Fig. 3.1. At each collision point, detectors are placed [43]. The ATLAS and the CMS (Compact Muon Solenoid) detectors are general purpose detectors for new discoveries and measurements. Together with the ALICE (A Large Ion Collider Experiment) and the LHCb (LHC beauty) experiments, which are constructed for specific phenomena, they are placed underground. A smaller experiment

called TOTEM (TOTAl Elastic and diffractive cross section Measurement) shares the collision point with CMS in the north part of the LHC ring. The LHCf (Large Hadron Collider forward) and the ATLAS detector sharing also a collision point are located on the opposite side of the ring in the south.

The efficiency of a collider is determined by the number of collisions produced per area and time - the luminosity. It depends on the number of protons per bunch, the time between the bunches, the cross section of the colliding bunches and the efficiency of the overlap of the cross sections. The integrated luminosity over the time delivered by the LHC is shown in Fig. 3.2 for the past years. In this project, data with a center of mass

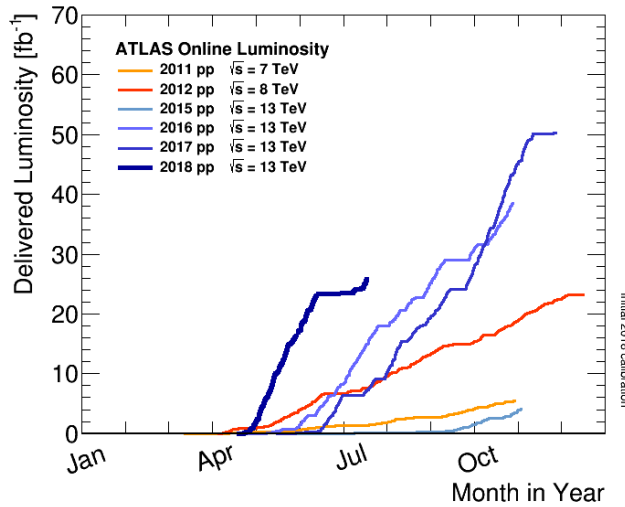


Figure 3.2: Delivered integrated luminosity per data-taking year [44].

energy of $\sqrt{s} = 13$ TeV are investigated. The search includes data from the run in 2015 with an integrated luminosity of 3.5 fb^{-1} and in 2016 with an integrated luminosity of 33.5 fb^{-1} . Both runs together provide a large data set with a total integrated luminosity of 37 fb^{-1} .

3.2 The ATLAS detector

The ATLAS detector is a particle detector in cylindrical shape at LHC. As the largest detector at a collider in the world, it has a diameter of 25 m, is 44 m long and weighs 7000 t.

3.2.1 Coordinate System

The ATLAS detector has a forward-backward symmetric cylindrical geometry. The incoming beam of the proton points along the z-axis in the cartesian coordinate system of the detector. In a right-handed coordinate system, the x-axis points to the center of the LHC ring and the y-axis to the top of the transverse plane perpendicular to the incoming beam. The origin is set to the collision point. This is illustrated in Fig. 3.3. The azimuthal angle Φ is the angle to the x-axis in the transverse plane. The polar angle Θ is measured with respect to the beam line along the z-axis. Transverse momentum p_T and

energy E_T that are measured in the xy-plane, are given by

$$p_T = \sqrt{p_x^2 + p_y^2} = p \sin \Theta \quad (3.1)$$

$$E_T = \sqrt{E_x^2 + E_y^2} = E \sin \Theta. \quad (3.2)$$

p_T is used to select events with at least two jets. The rapidity y of an outgoing parton is given by

$$y = \frac{1}{2} \ln \left(\frac{E + p_z}{E - p_z} \right). \quad (3.3)$$

The rapidity difference Δy between two outgoing parton y_1 and y_2 is given by

$$\Delta y = y_1 - y_2 \quad (3.4)$$

and is invariant under Lorentz Boost along the z-axis. For $E \ll m$ or $m \rightarrow 0$, the rapidity becomes η

$$\eta = -\ln(\tan(\Theta/2)) \quad (3.5)$$

which is also called pseudo rapidity. Then, the distance R between two objects is calculated by

$$R = \sqrt{(\Delta\eta)^2 + (\Delta\phi)^2}. \quad (3.6)$$

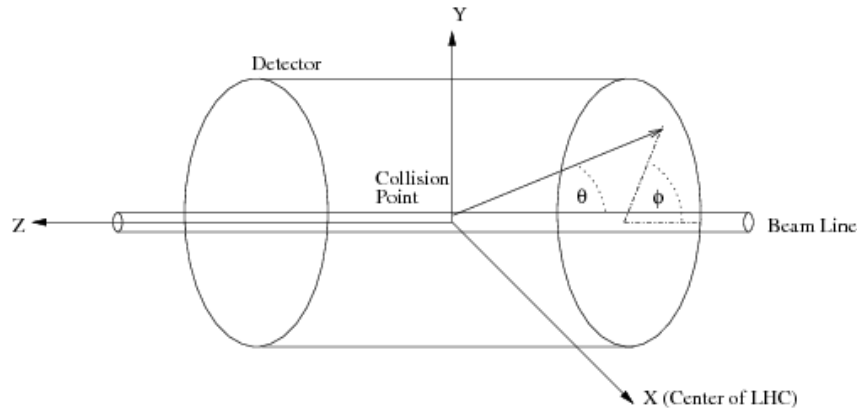


Figure 3.3: Coordinate system of the ATLAS detector [45]

3.2.2 Detector Components

The multipurpose ATLAS detector has several sub-detectors to measure different types of particles and their properties. The particles created by the collisions in the centre of the ATLAS detector are surrounded by different sub-detector layers over nearly the entire solid angle. A schematic sketch is shown in Fig. 3.4. Close to the center of collision, the inner detector is responsible for identifying the tracks of the charged particles. The inner detector is surrounded by the electromagnetic and the hadronic calorimeters. There, the energy of electromagnetically interacting particles (i.e. e^\pm, γ) and hadrons is measured. All particles which interact electromagnetically or strongly are stopped except for muons and neutrinos. The energy of the neutrinos cannot be measured in the entire detector since there is no component which captures neutrinos. The energy and momentum of muons is measured in the outermost layer, the muon spectrometer [2]. The sub-detectors responsible for the measurements are illustrated in Fig. 3.5 and described briefly in the following paragraphs.

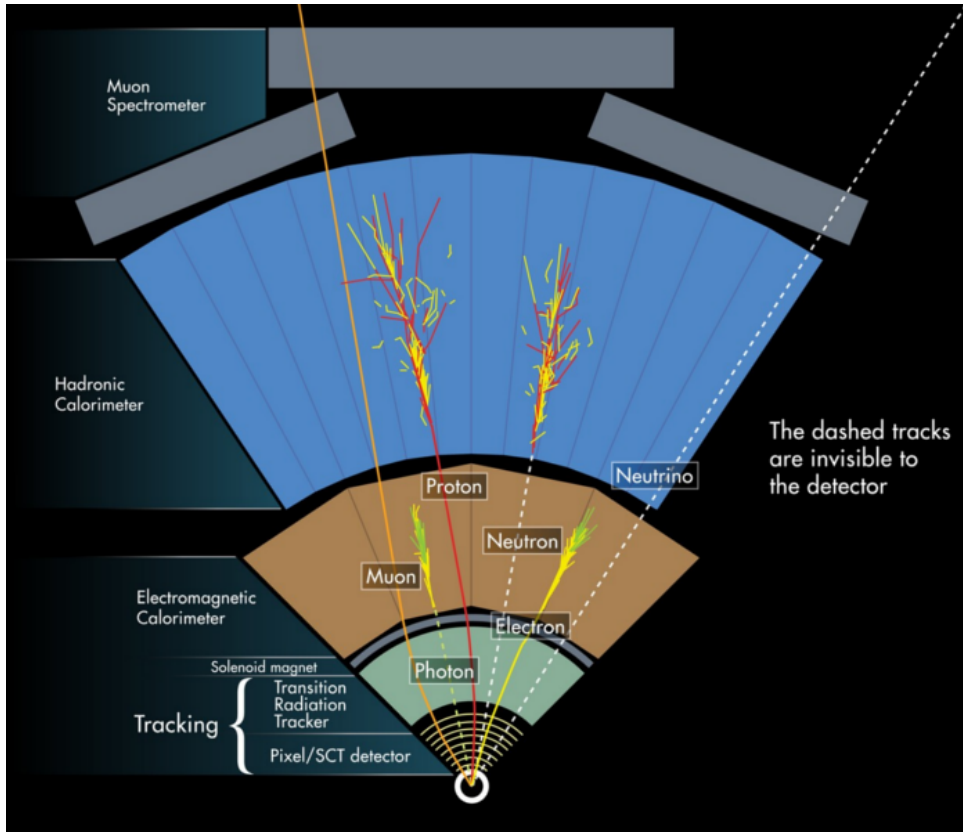


Figure 3.4: The layers in the ATLAS detector are shown [46].

Inner Detector The inner detector [48] measures the tracks of charged particles. A superconducting solenoid magnet bends the track of charged particles on the transverse plane to measure their momentum and to determine their charge. The inner detector consists of a pixel detector, a semiconductor tracker and a transition radiation tracker.

The pixel detector has four layers of pixels with 80 million silicon pixels in total, measuring the track of the particles accurately.

The pixel detector is surrounded by the Semiconductor Tracker which consists of eight layers of silicon micro-strip detectors. The eight layers provide eight independent, precise measurements of the momentum, the impact parameters and the vertex positions of the tracks.

The outermost sub-detector of the inner detector is the Transition Radiation Tracker consisting of 350.000 straw tubes filled with a Xenon and Argon gas mixture making a volume of 12 m^2 . It provides further tracking information on the particle type (i.e. whether it is an electron, positron or a charged pion).

Electromagnetic Calorimeter The electromagnetic (EM) calorimeter [49] absorbs the particles which interact only electromagnetically (i.e. e^\pm, γ). It consists of an EM barrel 5.6 m long and two EM end-cap calorimeters each 2.6 m long surrounding the inner detector. The EM barrel has three layers to record the position, the energy and the tail of the electromagnetic shower, respectively. The end-cap calorimeters consist of an outer wheel with two layers of modules and an inner wheel with three layers of modules. The EM calorimeter is a liquid Argon calorimeter with layers of liquid Argon as active material. The absorber material is lead.

The energy of a particle is measured by collecting the energy from all particles in the

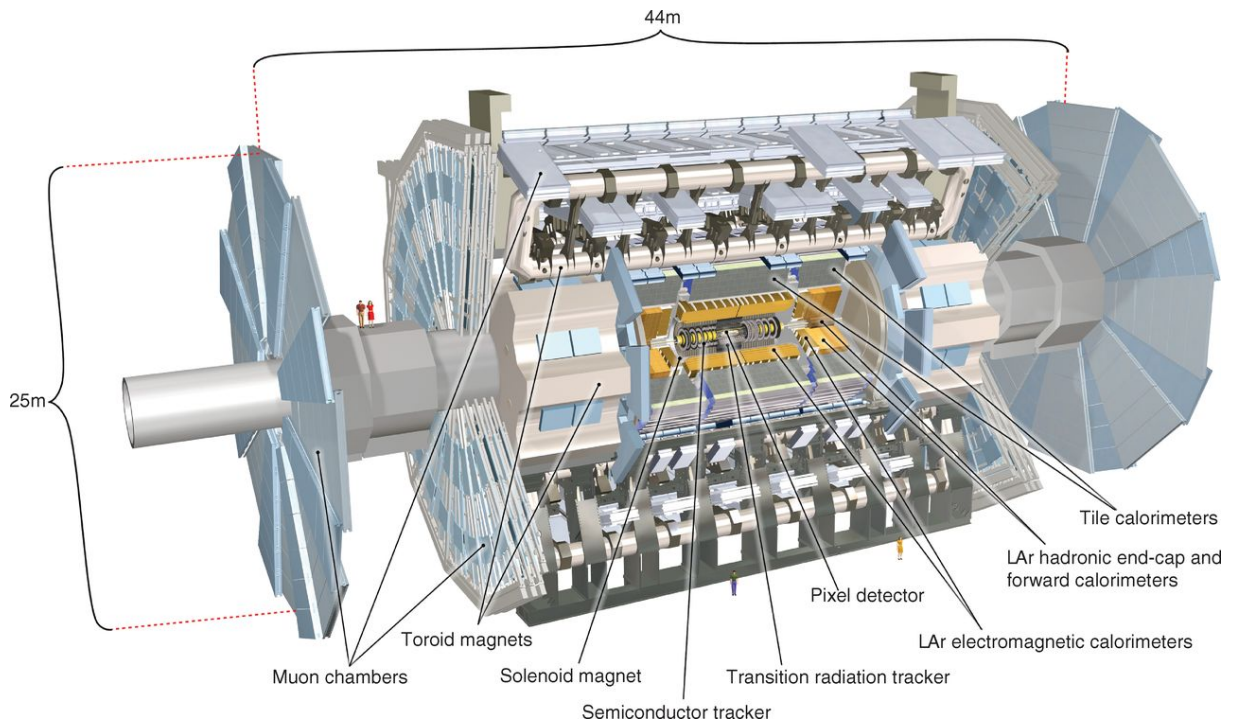


Figure 3.5: Components of the ATLAS detector [47]

EM showers, which were produced by the initial particle. EM showers [50] are created by high energetic electrons and positrons which lose energy due to bremsstrahlung by interacting with the absorber material in the detector. Photons are emitted producing e^-e^+ -pairs. If this pair has enough energy, the process starts from the beginning. Also, high energy photons can start an EM shower. For electron, positron or photon energies below 100 MeV, ionization of the detector material dominates and the EM shower ends. The active material in the EM calorimeter, liquid Argon, ionizes and emits electrons which produces a current between the electrodes of the lead layer. The current is proportional to the energy of the particle. The sum of the energies of all final particles creating a current, is proportional to the energy of the initial particle.

Hadronic Calorimeter The Tile calorimeter [49] is the hadronic calorimeter in the ATLAS detector. It consists of three sections: Two Tile extended Barrels surround a Tile Barrel. They are made of iron plates and plastic scintillator tiles. The scintillator radiates light if it is excited by a particle which is detected by a photo detector, which creates an electric signal amplified by a photo multiplier.

The particles interact with the absorber material in the calorimeter and hadronic showers are created. The particles in the shower activate the scintillator and the created electric signal is proportional to the energy.

Hadronic showers are created by hadrons. The following processes support the shower productions (c.f [51, 52, 53, 54]). By the hadronization of partons mostly pions are produced in the jet. The neutral pions decay into two photons ($\pi^0 \rightarrow \gamma\gamma$), which, in turn, start EM showers. In a nuclear reaction, excited nucleons N^* can lead to β^- or γ -decay via fission, to spallation or neutron capture can happen. Hadronic showers are quite complex and the ratios of the processes vary.

Energy resolution of calorimeters The energy resolution of a calorimeter is an important factor in determining the original parton energy. For known energy leakage, the measurements in the detector can be reconstructed and calibrated so that the energy difference between the real and the measured value becomes as small as possible.

Assuming a particle with the energy E . The number of particles N in a created shower is proportional to the energy (c.f. Ref. [53])

$$N \propto E. \quad (3.7)$$

The statistical fluctuations of the number of showers σ_N given by the Poisson statistic is

$$\sigma_N \propto \sqrt{N} \quad (3.8)$$

assuming all events are counted. The relative uncertainty of the energy due to statistical fluctuations is then given by

$$\frac{\sigma_N}{N} \propto \frac{\sqrt{N}}{N} = \frac{1}{\sqrt{N}} \Leftrightarrow \frac{\sigma_E}{E} \propto \frac{1}{\sqrt{E}}. \quad (3.9)$$

A proportionality constant A which considers fluctuations of e.g. the sampling, the leakage, electromagnetic fraction, nuclear excitation, in fission and the binding energy [54] is introduced. Besides the statistics, detector leakages, inhomogeneities, non-linearities and electronic noise change the result. Furthermore, a constant energy independent term B is introduced to balance e.g. shower leakages due to the geometry of the detector, inhomogeneities in the construction of the calorimeter, non-linearities for electronic readouts. The electronic noise depends with a proportionality of $1/E$ on the energy E . The factor C includes for example the readout electronic noise and pile-up fluctuations. These factors are all convoluted together to get the total energy resolution

$$\frac{\sigma_E}{E} = \frac{A}{\sqrt{E}} \otimes B \otimes \frac{C}{E}. \quad (3.10)$$

where E is given in [GeV].

For the ATLAS detector, the jet energy resolution is dependent on the rapidity η and is for A between 1.02 and 1.99, for B between 1.4% and 5.6% and C is not given [55].

Muon spectrometer Muons rarely interact in the calorimeter. The outer layer is therefore a muon spectrometer [56] in a toroidal magnetic field, which is created by the Toroid magnets. The muon spectrometer measures momentum of the muons by examining the curvature of the muon tracks in the toroidal magnetic field. In the muon chambers, there is a total of seven layers of Monitored Drift Tubes to identify the muon tracks.

4 Programming Tools

In this chapter, the programming tool Jupyter notebook is presented based on Ref. [4, 57]. The used packages and tools are described. Finally, a short description on how to run a Jupyter notebooks is given.

4.1 Project Jupyter and Jupyter notebooks

Jupyter notebooks are developed to provide an open source software for interactive data science and scientific programming by project Jupyter [57]. Project Jupyter is a non-profit organization that was founded in 2014 when the interactive computing environment IPython was adapted. Apart from editing the environments of IPython, Jupyter notebooks now also support further execution environments - so-called kernels - which allows the usage of other programming languages than Python in the interactive computing software. The three core programming languages **Julia**, **Python** and **R** coin the new name “Jupyter”. Today, over 40 programming languages are supported [4].

The Jupyter notebook is composed of cells. Cells are writing fields. The cells are connected so that the previous executed code is saved in the memory of the notebook. However, each cell is run individually. Using multiple cells makes the code more clear and gives it a better structure. The two main cell types are: a) a cell for coding called “coding cell” and b) a cell for documentation in form of rich text elements called “markdown cell”. Any number of cells can be used and for each the type can be chosen individually.

The main cell type is the coding cell. The cells enable to write and develop the code step-by-step. Debugging errors becomes easier. The output for each cell appears below the input e.g. for a code which creates a figure, the figure can be shown directly below the cell. Between the coding cells, it is possible to include rich text elements in the markdown cells. Texts in different formats, headings in different sizes and included pictures, videos and animations lead to a wide variety to formulate thoughts (e.g. about theory, explanations or interpretations) and to explain the code. Furthermore a $\text{L}^{\text{A}}\text{T}_{\text{E}}\text{X}$ -support is given to depict equations.

The Jupyter notebook programmed in this project uses the IPython kernel and the programming language Python 3. Python is a general purpose programming language which can be used for e.g. statistical data analysis.

4.1.1 Installation

For an offline use on the computer, the full installation of Jupyter notebook is recommended. Jupyter notebooks [58] can be either run via the Anaconda Distribution [59] or via Python’s package manager pip [60]. Then, run Jupyter notebook. Alternatively, the next generation of Jupyter notebooks JupyterLab [61] can be used for a more flexible environment. Further instructions are given on the homepage of Jupyter [57]. The python version used should be at least Python 3.

For an online use, several options are available. No installation is necessary by using the online interface TryJupyter with Python [62] or TryJupyterLab [63]. A cloud-based notebook is provided at SWAN@CERN [64]. All those ways can run Jupyter notebooks in the file format `.pynb`, which is also used in this project.

4.2 The Proof-of-Principle notebook using dijet events

The Proof-of-Principle notebook analyzing dijet events is created in order to make the theory, the experiment and especially the analysis of the dijet search [65] for new physics more readable, understandable and reproducible.

First, a Jupyter notebook in the programming language PyROOT [66, 67] was created based on Ref. [68]. This notebook needed a special environment to be executed. The installation was challenging using Windows as an operating system or using an online interface. Since, ROOT caused substantial problems for non-linux based operating systems outside an university network, the programming language was changed to Python 3 using `matplotlib.pyplot` for creating figures. The new Jupyter notebook version is easier to understand for beginners in programming without any knowledge in ROOT. No special packages must be installed. It can be easily run via all options described above.

The focus of the notebook is set on different ways for the visualization of the comparison of observed data with expected background in the dijet mass spectrum. Furthermore, the BumpHunter and the TailHunter algorithm, two hypothesis tests are applied. Lastly, a sanity check is performed, which shows that the results agree with the official results by the ATLAS Collaboration.

Content of the notebook The notebook starts with a general introduction about the theory behind the search. For more detailed information read the whole Section 2 about the theory. The SM is introduced by describing the elementary particles and their interaction. It is shortly mentioned how an excess would be created by a new resonant state. Then, the experimental tool, the LHC and the ATLAS detector are mentioned, that has recorded the data set used in this analysis. The idea of the analysis and the official figure with the results are presented.

After this very short introduction, the main part of the Jupyter notebook follows. The data and the background prediction are compared using different techniques. First, the data set is prepared to the notebook and saved into lists. The data structure and data analysis tool `pandas` [69] is used to read a `.csv`-file. The data is presented in the `pandas` tables. Visualizations of data and the background prediction are performed. Then, the bin-by-bin analysis is performed as described in Section 7.1. The following methods are applied:

- Absolute and relative difference (c.f Section 7.1.1)
- The Gaussian approximation of the significance (c.f Section 7.1.2)
- The significance (c.f Section 7.1.3)

The bin-by-bin analysis techniques are then compared. To do statistical calculations in the analysis, the package `statsmodel.api` [70] and `scipy.stats` [71] are used. With the plotting framework `matplotlib.pyplot` [72], the figures are created.

The bin-by-bin analysis is followed by the hypothesis hyper tests BumpHunter and TailHunter algorithm (c.f. Section 7.3.1). In the BumpHunter, sidebands are included which are also checked for excesses. An overview is given of the calculated p -values in the respective windows by a figure. Then, the distribution of the test statistics is shown. Similarly to the BumpHunter, the TailHunter is implemented. Also, the windows with their p -values and the TailHunter test statistic distribution are included. Lastly, the results are presented.

4.2.1 Usage

Preparation To use the Proof-of-Principle notebook, the program “Jupyter notebook” should be installed as described in Section 4.1.1 or the online interface should be opened.

The notebook file of this project is called `ProofofPrincipleNotebook_v1.ipynb` and the corresponding data set is `HEPData-ins1519428-v2-Table1.csv` which can be downloaded in Ref. [73]. For the further procedure it is important that both files are always saved in the same directory either on the computer or on the online interface. That means that they must be in the same folder and the name should not be changed for the usage.

TryJupyter In order to use the online interface TryJupyter, go to jupyter.org/try, and select *TryJupyter with Python*. Then, wait until the binder has loaded the Jupyter notebook called “Index”. Now, the file `ProofofPrincipleNotebook_v1.ipynb` should be opened there. Go to *File* on the left top and select *Open... .* A new window should pop up which shows some files in a directory. Click on *Upload* on the right top and upload both files, `ProofofPrincipleNotebook_v1.ipynb` and `HEPData-ins1519428-v2-Table1.csv` by selecting and opening them. Once you have selected them, you need to click on the blue button *Upload* to finally upload the files. Now, `ProofofPrincipleNotebook_v1 .ipynb` can be opened and the notebook be used.

TryJupyterLab The alternative to TryJupyter is the online interface TryJupyterLab. On the homepage jupyter.org/try select *Try JupyterLab*. Click on the symbol which is marked as *Upload Files*. Then select both files, `ProofofPrincipleNotebook_v1.ipynb` and `HEPData-ins1519428-v2-Table1.csv`. They should appear in the directory on the left hand side. By clicking on `ProofofPrincipleNotebook_v1.ipynb`, the notebook opens on the right hand side and is ready to use.

SWAN@CERN As a member of CERN, one has the access to the online cloud-based tool called SWAN@CERN. Go to <https://swan.cern.ch> and log in with you account details. A “Starting SWAN” screen appears which can load for a little while. On the right hand side, a window with “Configure Enviroment” appears. Change only the Software Stack to *93 Python 3*. Then, click on the blue button with *Start my Session*. Click on the “Plus” symbol the right top and add a new project by creating a new folder. The folder opens automatically. With *Upload file*, `ProofofPrincipleNotebook_v1.ipynb` and `HEPData-ins1519428-v2-Table1.csv` can be uploaded by selecting them and clicking on the blue *Upload* button.

Jupyter notebook and JupyterLab After the installation, open the program Jupyter notebook as described in Ref. [58]. Then, a directory with the files on your computer opens in your standard internet browser. There, you should go into the folder where both files are saved and click on the Jupyter notebook file ending with `.ipynb` to open it.

Running the notebook As described earlier, the notebook is made of coding and markdown cells. The markdown cells should be are already executed. If not, do it like the coding cells. The coding cells can be executed by pressing SHIFT and ENTER or STRG and ENTER at the same time. The difference between those two methods is that

the selection of the cell keeps for STRG+ENTER and for SHIFT+ENTER the next cell is selected.

It is important, that the cells are executed in the correct order. The hierarchy of the cells are to be maintained. The reason for this is that variables are defined in the beginning and then used in several following cells. By the violation of the order of the executed cells, it can come to error messages and the notebook does not work properly. In that case, starting the execution of each cell from the beginning can help.

In the code, comments are included to document the code and explain the steps in the code. They are marked with the number sign “#” as shown below.

```
# This is an example for a comment.
```

If the notebook is run with JupyterLab, one should use `%matplotlib inline` in order to show the plots below the executed cell. With Jupyter, it is possible to have interactive figures with `%matplotlib nbagg`. An example is shown in Fig. 4.1. `nbagg` enables to zoom in the spectrum or to change the range in the spectrum. This can be regulated with the buttons on the left bottom side. With `g`, a reset to the original view is performed, `d` goes back to the previous view, the arrow showing to the right side forwards to the next view. By clicking on the box, a part of the figure can be selected which is the zoomed in. The figure can be saved by clicking on the symbol on the right hand-side.

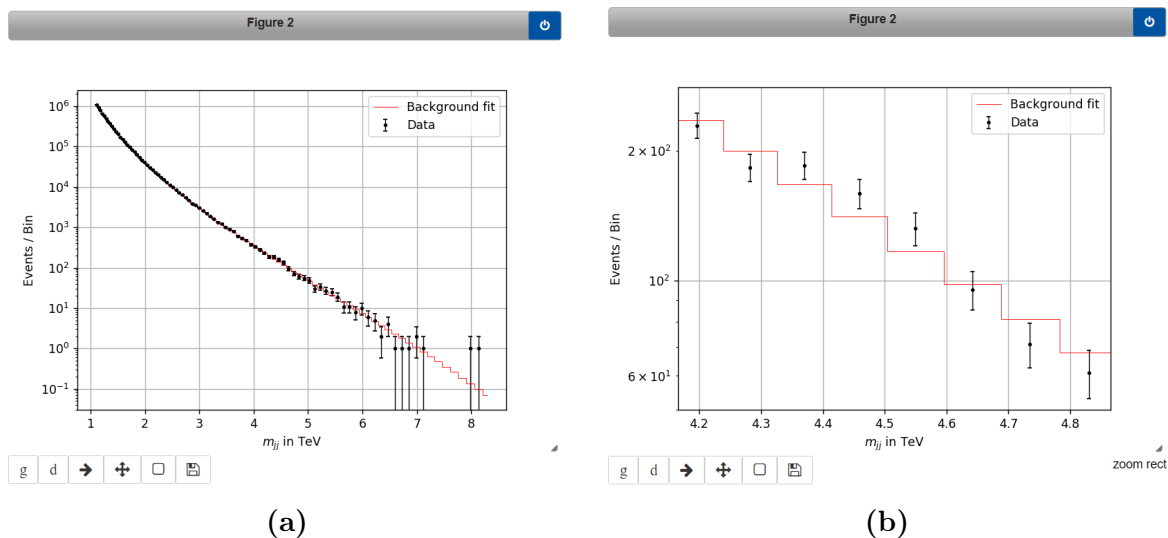


Figure 4.1: Example for using `%matplotlib nbagg`.

Optional features In this notebook, additional optional features are included. It is not necessary to use the optional features however they can be a useful addition. An optional feature could be for example that the elements in the figure can be easily added or adjusted.

The optional features are marked with “Optional” and are excluded in the main code with the number sign `#`. By removing the number sign `#` in the following lines of the describing line, the optional feature is applied the next time when the cell is executed. By adding the number sign `#` again and executing the cell, the optional feature is not

active anymore. The example below shows how a text can be added to a figure through an included optional feature. Here, general information about the data set is given. The two numbers in `ax.text()` determine the position of the text while the first number gives the x and the second number the y position. This is followed by a text in quotation marks which will appear in the figure.

```
 #(Optional) Add text with further information about the plot
#ax.text(1,10**0+1,'Center of mass energy:$\sqrt{s}=13\,$TeV')
#ax.text(1,10**(-1)+10**(-.5),'$L_{\text{int}}\$=37.0\text{fb}\$^{-1}\$')
#ax.text(1,10**(-1),'Run in 2015 and 2016')
```

```
 #(Optional) Add text with further information about the plot
ax.text(1,10**0+1,'Center of mass energy:$\sqrt{s}=13\,$TeV')
ax.text(1,10**(-1)+10**(-.5),'$L_{\text{int}}\$=37.0\text{fb}\$^{-1}\$')
ax.text(1,10**(-1),'Run in 2015 and 2016')
```

Using another data set The notebook is so constructed that other text files in the csv-format can be used. In order to use another data set, some parts of the code must be adjusted. There are two components in the code which read and select the data from the data file. How to adjust those is explained and shown below.

```
 # Adjust the name of the file and of the columns
data = pd.read_csv("newdataset.csv", names=["column1",
"column2","column3","column4"])
temp = pd.concat([data])
temp[10:102].style # Adjust
```

Firstly, the complete file is read with the command `pd.read_csv` where "newdataset.csv" is the name of the data file and in `names=[...]` the columns are related to a name. In this example, the first four columns are read into the variable `data`. If there are more columns to read, this should also to be adjusted. Now, all lines in each column are imported. If any lines should be ignored, this can be done as shown below.

For the column `columnX` in `data`, the values between the lines, here 10 and 102, `[10:102]` are related to the variable `y`. The lines can be adjusted. Optimally, the name of the final variable should be kept and the columns related correspondingly.

```
 # Measured Events/Bin
y = [float(i) for i in pd.Series(data["columnX"]
[10:102]).values.tolist()] # Adjust
```

BumpHunter and TailHunter The BumpHunter and the TailHunter algorithm are hyper hypothesis tests that are implemented in the notebook. Both investigate the differences between measured data and the background prediction in different part of the spectrum called windows. Both algorithms do have parameters influencing the accuracy

and the calculation time. In order to get more precise results or to reduce the calculation time, the adjustment the parameters is described below.

Sidebands Sideband are defined as the regions left and right next to the window. The sideband criteria investigated whether the window is a significant region. Usually, sideband criteria is included in the BumpHunter algorithm however this extends the calculation time. In the BumpHunter algorithm implementation, one can switch between considering sidebands or not by changing `evaluate_sidebands` with `evaluate_statistic` or the other way around. This should be only done in the part of the BumpHunter code for the data and the pseudo data shown below. Do not change the name when the function is defined.

```
# Creating pseudo experiments and obtain their test statistic
# Pseudo data investigated with sidebands
pseudo_experiments = [evaluate_sidebands(pe, bkg)[0]
                       for pe in make_toys(bkg, n)]
# Determine the test statistic for the data set (measurements)
# Data investigated with sidebands
measurement,(lo, hi),window,pval = evaluate_sidebands(data,bkg)
```

The implementation with sidebands can be changed to

```
# Creating pseudo experiments and obtain their test statistic
# Pseudo data investigated without sidebands
pseudo_experiments = [evaluate_statistic(pe, bkg)[0]
                       for pe in make_toys(bkg, n)]
# Determine the test statistic for the data set (measurements)
# Data investigated without sidebands
measurement,(lo, hi),window,pval = evaluate_statistic(data,bkg)
```

Pseudo experiments Pseudo experiments are created in order to determine the probability to wrongly rule out the background prediction called p -value. The number of pseudo experiments is essential for the accuracy of the p -value. In the notebook, the number of pseudo experiments is chosen to be 10000. A higher number of pseudo experiments lead to a higher precision and a higher calculation time. The number 10000 can be replaced for the BumpHunter and the TailHunter as shown below.

```
# 10000 pseudo experiments for the BumpHunter algorithm
test,t, edges, mjjudge, pvalue, puncertainty,
    window, pval = bumphunter(x, y, yb, 10000)

# 10000 pseudo experiments for the BumpHunter algorithm
testtail, ttail, edgestail, pvaltail = tailhunter(x,y,yb,10000)

# Choosing 50000 pseudo experiments for the BumpHunter algorithm.
test,t, edges, mjjudge, pvalue, puncertainty,
```

```
    window, pval = bumphunter(x, y, yb, 50000)

# Choosing 1500 pseudo experiments for the TailHunter algorithm.
testtail, ttail, edgestail, pvaltail = tailhunter(x,y,yb,1500)
```

5 Selection and Background Estimation

With the ATLAS detector at the Large Hadron Collider (LHC) at CERN, proton-proton collision events at a center of mass energy of $\sqrt{s} = 13$ TeV are investigated for the presence of new resonances decaying into dijets. The search includes data from the run in 2015 with an integrated luminosity of 3.5 fb^{-1} and from 2016 with an integrated luminosity of 33.5 fb^{-1} . Both runs together provide a data set with a total integrated luminosity of 37 fb^{-1} .

The reconstruction of jet events in the data set is described in this chapter. Reconstruction is the procedure how the identification of particles is performed on the basis of the electronic signals. Following, the calibration procedure which corrects the physical properties of the measured jets like the momentum and energy including the detector attributes is described [74, 75, 76, 77, 78]. Then, the selection criteria are shown. In the last part of this chapter, the fitting method for the background estimation [79] is introduced.

5.1 Reconstruction of Jets

The hadronisation of parton produces collimated showers of particles called jets. For the reconstruction of jets, particles from the parton shower are clustered together. The kinematics of the reconstructed jet are nearly those of the initial parton.

The calorimeters consist of many cells. The transverse momentum p_T of a jet is determined by summing up all energy measurements belonging to the same jet. For this, the calorimeter cells are collected into groups of energy deposits called topological clusters. The construction procedure of the topological clusters is described in Ref. [80]. The energy of each topological cluster E_{cluster} is calculated by summing up the energy of each calorimeter cell in the cluster. Then, the directions $(\eta_{\text{cluster}}, \phi_{\text{cluster}})$ relative to the center of the ATLAS detector are calculated by taking the direction of each cell $(\eta_{\text{cell}}, \phi_{\text{cell}})$ weighted by the energy of each cell with the total energy of the cluster. The jet clustering algorithm determines the jets on the basis of the topological clusters with a transverse momentum calculated by E_{cluster} , η_{cluster} and ϕ_{cluster} . The anti- k_t algorithm [81] with the radius parameter $R = 0.4$ [3] is used to reconstruct the jets. The algorithm is based on the distance parameter $d_{i,j}$

$$d_{i,j} = \min \left(p_{T_i}^{-2}, p_{T_j}^{-2} \right) \frac{\Delta_{i,j}^2}{R^2} \quad (5.1)$$

between the object i and the object j which are topological clusters. The separation $\Delta_{i,j}$ is calculated with $\Delta_{i,j}^2 = (y_i - y_j)^2 + (\phi_i - \phi_j)^2$ with the rapidity y and the azimuthal angle ϕ . The object-beam distance $d_{i,B}$ is set to $d_{i,B} \equiv p_{T_i}^{-2}$. $d_{i,B}$ and $d_{i,j}$ are calculated for all clusters measured in the calorimeter. With $d_{i,j}$ as the smallest distance, the corresponding clusters are combined to one cluster counting as a new cluster. This is repeated until $d_{i,B}$ becomes the smallest calculated distance. Then, the cluster i is defined as a jet and removed from the considered clusters. The distances are re-calculated and the algorithm continues until all clusters have been associated to a jet.

For a reconstructed jets, their energy and momentum is calculated using the four-vector recombination scheme [82]. The four-vector momentum of a jet is determined by summing up the four momentum of all objects belonging to the jet.

Then, the ghost association technique [83] is applied to relate the tracks of the particles to the jets.

5.2 Calibration of Jets

In the topological clusters, not all of the four momentum is measured. Reasons are on the one hand detector effects like inactive material, the lower response of the detector to hadronic showers, particles of the jet outside the detector (jet punch-through), noise thresholds, and pile-up effects [84, 65]. A missing transverse momentum is problematic if new discoveries are expected. Therefore, the jet energy response (the difference between the measured jet energies to their true value) and the resolution (JER) need to be well understood. To ensure this, a calibration of the jets is performed. The jet energy scale (JES) is restored in several steps as explained in Ref. [75]. An overview of the calibration procedure is given in Fig. 5.1.

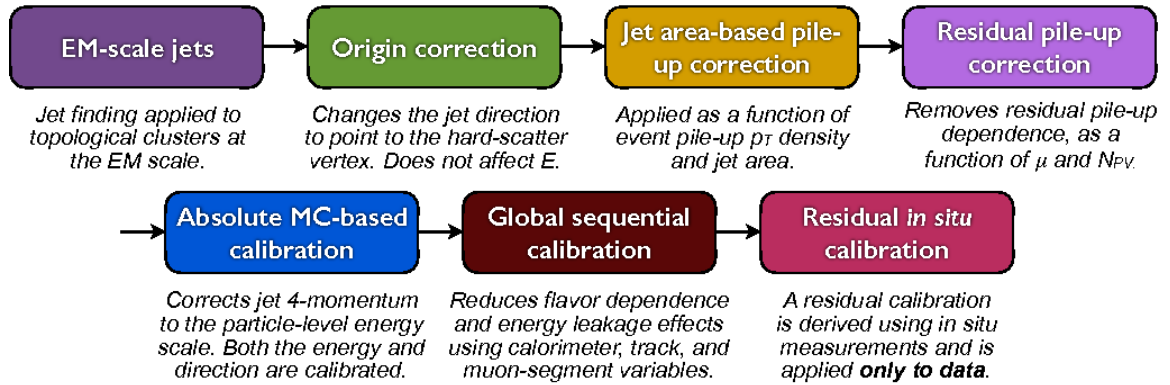


Figure 5.1: Calibration stages with a short explanations for EM-scale jets [65].

The steps are shortly introduced here starting from reconstructed jets to the electromagnetic (EM) scale [84].

1. **Origin correction:** The direction of the jets are corrected that the four-momentum points to the primary vertex of the interaction. This correction does not affect the energy E of the jet. However, the resolution in η of the jet is improved.
2. **Pile-up offset correction:** The corrections for pile-up effects are applied: One correction is event-based. The p_T density of the pile-up collisions in the event is determined. Together with the jet area a correction is applied to the p_T of the jet. Another correction based on the number of primary vertices and the average interactions per bunch crossing is applied to the p_T of the jet.
3. **Absolute MC-based calibration:** The four-momentum and the pseudo-rapidity η of a jet are corrected to the particle level jet scale using MC simulations. A particle level jet is built by hadrons stemming from only hard scattering processes with a proper mean decay length of $c\tau > 10$ mm with the life time τ . The average energy response $R(E_{\text{reconstructed}})$ between the energy of the reconstructed to the truth jets in the MC

$$R = \left\langle \frac{E_{\text{reconstructed}}}{E_{\text{truth}}} \right\rangle$$

is used to determine a calibration factor. The numerical inversion technique is applied to calculate the values of $E_{\text{reconstructed}} = R(E_{\text{truth}}) \cdot E_{\text{truth}}$. Then, the calibration factor is obtained by fitting $R(E_{\text{reconstructed}})$.

4. **Global sequential calibration:** The jet reconstruction is sensitive to the jet particle composition and the distribution of energy within the jet. These properties can vary between different initiating partons, e.g. quark initiated versus gluon initiated jets.

To reduce the dependencies of the Jet Energy Scale (JES) on these differences, corrections are applied which are based on sensitive variables from the calorimeter, the tracker and the muon system.

5. **Residual in situ calibration:** The last step is the residual in situ calibration which corrects the fact that MC cannot represent data perfectly. The residual calibration uses in situ measurements which are derived from collision data as described in Ref.[85]. The Jet Energy Scale (JES) is calculated by

$$\text{JES}^{in\ situ} = \frac{\langle p_T^{\text{jet}}/p_T^{\text{ref}} \rangle_{\text{MC}}}{\langle p_T^{\text{jet}}/p_T^{\text{ref}} \rangle_{\text{data}}} \quad (5.2)$$

as the ratio between the average transverse momenta of the calibrated jets to reference objects (e.g. photons, Z bosons, or other jets) of the MC jets and the jets in the data. To get this ratio, three corrections are performed:

- (a) **Relative η inter-calibration:** Correction of the jet response for forward jets ($|\eta| > 0.8$) balanced to dijets in the central region ($|\eta| < 0.8$).
- (b) **Absolute p_T -calibration:** Photons and Z-bosons are used as reference objects for the calibration of low energy jets in the central region.
- (c) **Calibration of high p_T jets:** Since photons and Z-bosons have to less energy, well calibrated, low p_T jets are used as reference objects for the calibration using the multijet balance method [86].

Those three steps are then combined and applied only to the data.

Jet energy scale uncertainty

The JES uncertainty [3] is derived with in situ studies for central jets containing the uncertainties in the calibration. This includes amongst others uncertainties of MC, the reference objects, pile-up, jet punch-through. For high p_T jets, the size of the event sample is too small that other methods are used. Here, single-particle response measurements [87] determine the uncertainty.

Including more than 70 nuisance parameters [16] yields a uncertainty function of p_T with 1% uncertainty for $p_T = 500$ GeV and 3% for $p_T = 2$ TeV [3].

Jet Energy Resolution

The JER [76] is determined by fitting

$$\frac{\sigma(p_T)}{p_T} \quad (5.3)$$

with a Gaussian function to calculate the p_T response distribution. Then, the root mean square (rms) of the fit $\sigma(p_T)$ and the mean value $\langle p_T \rangle$ are calculated. The JER is then

given by

$$\text{JER} = \frac{\text{rms}}{\langle p_T \rangle}. \quad (5.4)$$

The JER uncertainty is derived from simulations of QCD processes as further described in Ref. [77]. With a center of mass energy of 13 TeV, uncertainty due to JER for a dijet mass of 2 TeV is 2.4% and for 5 TeV 2.0%. The uncertainty has a negligible effect on the analysis [3].

5.3 Selection criteria

This section describes the selection of data, so that good functioning of the detector is ensured, and that resonance dijet events are chosen based on Ref. [88].

The Data Quality (DQ) group has developed a list called 'Good Run List' (GRL) which gives DQ information about a data set. The recorded data set is checked by the GRL. Only data that was recorded, while all ATLAS subdetectors were fully functional, is considered in the analysis.

In addition, event level quality requirements are applied. Events are discarded, if noise or corruption are present in the calorimeter. The remaining events are saved if they activate the lowest- p_T -singlejet-trigger. Those events have at least one jet with

$$p_T > 380 \text{ GeV}$$

after the reconstruction by the trigger.

For the offline analysis, only events are selected which have at least

- (a) a leading jet with $p_T > 440 \text{ GeV}$
- (b) a sub-leading jet with $p_T > 60 \text{ GeV}$
- (c) $m_{jj} > 1.1 \text{ TeV}$ (c.f. Eq. (2.1)).

This selection ensures that the trigger efficiency is high with at least 99.5% for central jet events [89] as shown in Fig. 5.2.

The selection is controlled by studying jet timing. Jet timing investigates whether the jet is produced by hard scattering or by other processes. So-called "fake" jets are created for example by the calorimeter noise in the Hadronic End Cap calorimeter, by background induced from other pp -collisions in the bunch or by non-collision backgrounds from cosmic-ray showers. With the jet timing criteria called "BadLoose" criteria given in Ref. [88], likely fake jets are excluded with a high efficiency over 99.5%.

For the resonance analysis, specific cuts are performed. To reduce the amount of SM QCD processes in the model independent search, a cut on the rapidity difference

$$y^* = \frac{y_1 - y_2}{2} \quad (5.5)$$

between two outgoing partons y_1 and y_2 is applied:

$$|y^*| < 0.6 \quad (5.6)$$

calculated with Eq. (3.4) and Eq. (3.3). In this choice, the benchmark models presented in Section 2.3 are constrained. Since the excited quark q^* , QBH, the W' and Z' boson

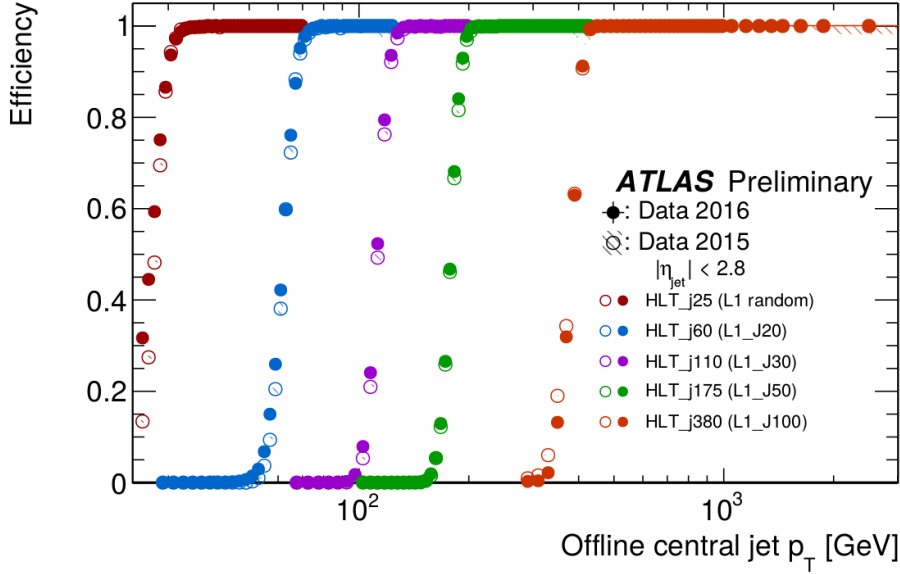


Figure 5.2: The trigger efficiency is shown for different p_T threshold triggers. The trigger HLT_j380 for the leading jet $p_T > 380$ GeV is marked in orange. The plateau of the high efficiency is reached for a central jet with $p_T > 400$ GeV [89].

have in a dijet production their distribution peak at $|y^*| = 0$. Here, the jets are centrally distributed. The W^* benchmark model has a very low selection efficiency peak at $|y^*| > 1$.

After the event selection, the lowest considered invariant dijet mass is $m_{jj} = 1.1$ TeV. The analysis spectrum extends to the highest measured invariant dijet mass at $m_{jj} = 8.12$ TeV. The binning of the m_{jj} distribution is chosen that the bin widths

- (a) approximate the m_{jj} resolution. The bin widths must be equal or greater than the m_{jj} resolution. For an increasing mass, the resolution decreases. Thus, the bin width gets wider.
- (b) are so small that the maximal number of bins is reached to get a higher resolution in the spectrum. The narrowest possible bin width ensures that it is smaller than the expected signal width.
- (c) are chosen, such that the smoothly decreasing background predicted by QCD is ensured.

Considering all requirements, the bin widths are chosen to be between 130 GeV and 180 GeV depending on m_{jj} given in Ref. [73].

5.4 Background estimation

While many analyses use simulated events to estimate the background, for the dijet analysis this method is not practical since QCD processes are difficult to model. Therefore, another strategy is chosen which was performed also in previous dijet resonance searches [90, 91, 92, 93, 94, 95, 96, 97]. A smooth fit is performed to estimate the background. A monotonically falling function

$$f(x) = p_1(1-x)^{p_2}x^{p_3}x^{p_4 \ln x}x^{p_5(\ln(x))^2} \quad (5.7)$$

with up to five free parameters p_i is used. Here x is given by $x = \frac{m_{jj}}{\sqrt{s}}$, with the invariant dijet mass m_{jj} and the center of mass energy \sqrt{s} . Depending on the properties of the data (e.g. the fit range, data set size), the number of the parameters p_i can freely be chosen. If the number of free parameters is too small, the background function is not accurate enough to describe the data. On the other hand, if the number of free parameters is too large, the fit function becomes too flexible and potential excesses could be hidden.

More parameters in the function are required if the data is statistically precise. For a large precise data set as used in this search, it is therefore unpractical to perform a single global fit. Thus a new sliding window technique is applied.

The new method called Sliding Window Fits (SWiFt) was developed to fit the background in a reasonable way. In this technique, the spectrum is fitted in restricted regions, in smaller ranges called windows. This gives the fit a higher flexibility. The window sizes are chosen so that the fit function (here three parameter, called nominal ansatz)

$$f(x) = p_1(1-x)^{p_2}x^{p_3} \quad (5.8)$$

describes it well. The window size is approximately half of the total numbers of bins. This is determined using a method described in Ref. [79]. The windows slides across the spectrum in small steps so that the windows are still overlapping. This method ensures that a potential signal is not fitted. The background fit becomes a smooth function. In every window fit, the bin center is evaluated and chosen for the total window fit. For the regions of the left and right edge, the window size is reduced up to 60% of nominal window size to evaluate the bin center. For the residual bins near the edge which have not been a bin center yet, the background values for of the window with 60% of nominal window size are taken for the final background fit. That means that the background is constructed bin-by-bin by a full set of windows which cover the complete mass range, here from 1.1 TeV to the highest observed dijet mass at 8.12 TeV. Compared to a global fit with e.g. the four parameter fit function on the whole spectrum, the new technique is also consistent to the data and more appropriate than a global fit. The resulting background fit is shown in Fig. 5.3.

One uncertainty of the total fit comes from determining the parameters p_i in the fit functions through the fit, respectively for each bin. To estimate the impact of this, pseudo data is generated under background prediction. On the different sets of pseudo data, the sliding-window procedure is repeated. The uncertainty on the number of events n in a m_{jj} bin is calculated by the root mean square of all pseudo experiments.

Another uncertainty factor arises from the choice of the fit function. An additional SWiFt is performed with the four-parameter fit function

$$f(x) = p_1(1-x)^{p_2}x^{p_3}x^{p_4 \ln x} \quad (5.9)$$

called alternate fit. The nominal fit is then compared to the alternate fit. On the prediction of the nominal fit, a set of pseudo experiments is created. These pseudo data set are fitted with the nominal fit (3 parameter) and with the alternate fit (4 parameter) by the SWiFt. Then, the difference between the background values for each bin are calculated. The average of all created pseudo data

$$\Delta x = \frac{1}{n} \sum_{i=1}^n |x_{\text{nominal}} - x_{\text{alternate}}| \quad (5.10)$$

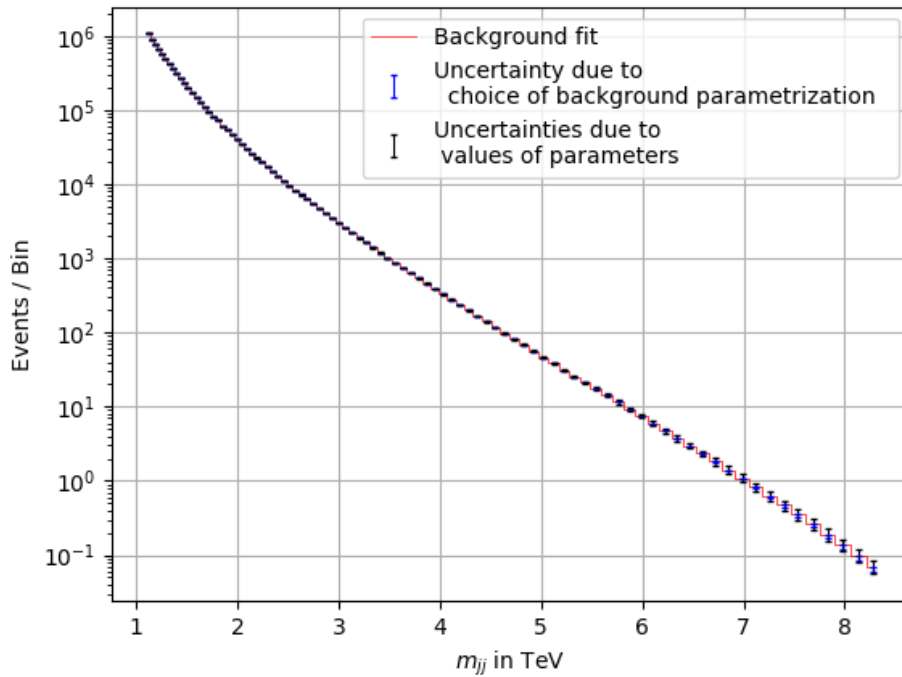


Figure 5.3: The result of the background fitting method (cf. Ref.[98]) with uncertainties is shown. A smooth function without any bumps is determined.

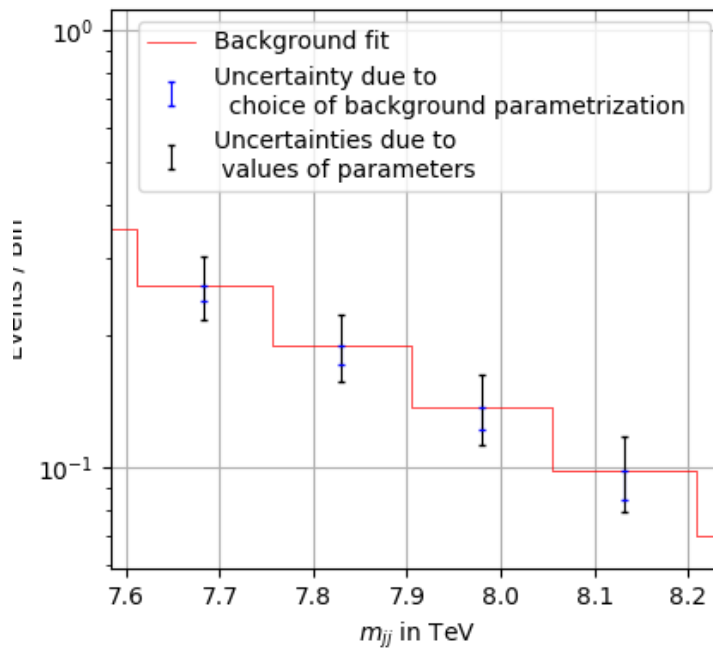


Figure 5.4: The background and its uncertainties are zoomed in in the m_{jj} range 7.6-8.2 TeV. The uncertainty due to the choice of the background parametrization is shown in blue and the uncertainty due to the values of the parameters is given in black.

is the uncertainty for each bin respectively. Both systematic uncertainties are given in Tab.1 of Ref. [98] and in Fig. 5.3. A zoom of Fig. 5.3 in order to see the uncertainties from Tab.1 of Ref. [98] in the range of high m_{jj} is shown in Fig. 5.4. The uncertainties are so small that they will not be shown in the following figures with the background prediction.

6 Basic Principles of Statistics

The basic concept of statistic relevant for the data analysis is presented [99]. The measurement of the number of dijet events [3] is a counting experiment which can be described through probability models. The binomial, Poisson- and Gaussian probability distributions are introduced. The data of Tab.1 in Ref. [3] follows a Poisson distribution as explained in this chapter. The second part of this chapter gives a short introduction into statistical hypothesis testing [5].

6.1 Probability models for counting experiments

This section is based on Ref. [99]. For counting experiments with independent events and two different outgoings, the probability distribution can be described by a binomial distribution

$$P(x|N, p) = \binom{N}{x} p^x (1-p)^{N-x} \quad (6.1)$$

with the number of trials N , success events x , and the success probability p . It gives the total success probability that x events out of N trials occur if x succeeds with the probability p . The expectation value is given by $\mu = Np$ and the variance by $\sigma^2 = Np(1-p)$.

For a large number of events N and $p \ll 1$ but $\mu = Np = \text{const}$, the binomial distribution is approximated by the Poisson distribution (c.f. Appendix A.1.1). Another ansatz to calculate the Poisson distribution is shown in Appendix A.1.2.

The resulting probability mass function for the Poisson distribution is given by

$$P(x|\mu) = \frac{1}{x!} \mu^x e^{-\mu}. \quad (6.2)$$

with the number of observed events x and the expectation value $\mu = N \cdot p$

$$\lambda = \sum_{x=0}^{\infty} x P(x) = \sum_{x=0}^{\infty} x \frac{e^{-\mu} \mu^x}{x!} = \mu \cdot e^{-\mu} \sum_{x=1}^{\infty} \frac{e^{-\mu} \mu^{x-1}}{(x-1)!} = \mu \quad (6.3)$$

which is constant. The variance of this discrete probability distribution is calculated by σ^2

$$\begin{aligned} \sigma^2 &= \sum_{x=0}^{\infty} x^2 P(x) - \left(\sum_{x=0}^{\infty} x P(x) \right)^2 = \mu \cdot e^{-\mu} \sum_{x=1}^{\infty} x \frac{e^{-\mu} \mu^{x-1}}{(x-1)!} - \mu^2 \\ &= \mu \cdot e^{-\mu} \left(\sum_{x=1}^{\infty} \frac{e^{-\mu} \mu^{x-1}}{(x-1)!} + \mu \cdot e^{-\mu} \sum_{x=2}^{\infty} \frac{e^{-\mu} \mu^{x-2}}{(x-2)!} \right) - \mu^2 \\ &= \mu^2 + \mu - \mu^2 = \mu. \end{aligned} \quad (6.4)$$

The standard deviation is then $\sigma = \sqrt{\mu}$.

For a large number of observed events x , the Poisson distribution can be approximated by the Gaussian distribution Appendix A.2

$$P(x|\mu, \sigma) = \frac{1}{\sqrt{2\pi\sigma^2}} \cdot e^{-\frac{(x-\mu)^2}{2\sigma^2}} \quad (6.5)$$

with the expectation value μ and the variance $\sigma^2 = \mu$.

To describe the data set Tab.1 in Ref. [3] with a probability distribution, the Poisson distribution is the best ansatz. For that, the number of events in each bin x is considered. The number of total events N in all bins is high with in total $N = 6462845$ events so that most bins are high populated. Only a few low populated bins cannot be described properly by the Poisson distribution. However, this is negligible.

6.2 Statistical Hypothesis Testing

This chapter introduces into statistical hypothesis testing. Statistical methods are explained which make a statistical decision about the agreement between data and a prediction called hypothesis. Firstly, the operation of a general hypothesis test is described in Section 6.2.1. Then, the two types of hypothesis tests, which are performed in this project are depicted: A hypothesis test which compares data and hypothesis bin-by-bin and global hypothesis hyper tests called BumpHunter and TailHunter algorithm. This chapter is based on Ref. [5, 6].

A hypothesis test is a test which checks whether a set of data D is consistent with a hypothesis H_0 . The test specifies either, whether the hypothesis is rejected or retained. In the case of rejection, the data is not consistent with the hypothesis or there is an evidence against H_0 . The data do not contradict to H_0 if the hypothesis is retained.

6.2.1 General operation of a hypothesis test

Given are data D and a prediction called hypothesis H_0 . A hypothesis test introduces a new parameter called test statistic t which is dependent on the value of D and H_0 . Depending on the hypothesis test, t is defined differently. However it follows the principle that the test statistic t is higher for larger discrepancies of D and H_0 .

In the second step, pseudo experiments are generated which are following the distribution of H_0 . The test statistic t is calculated for all pseudo experiment according to H_0 . A distribution of test statistics t is generated.

Then final step is to calculate the p -value. It gives the probability that the hypothesis H_0 is wrongly ruled out and is defined as

$$p\text{-value} = P(t \geq t_0 | H_0).$$

It is the probability to find the same or a higher test statistic t than t_0 in a pseudo experiment if H_0 is true. It is evaluated by the probability density function $\rho(t|H_0)$

$$p\text{-value} = P(t \geq t_0 | H_0) = \int_{t_0}^{\infty} \rho(t|H_0) dt. \quad (6.6)$$

For a non-continuous probability function, the p -value is estimated by counting all $t \geq t_0$ in the distribution. The total number of pseudo experiments N and the number of pseudo experiment S which fulfill the requirement, determine the p -value as

$$p\text{-value} = \frac{S}{N}. \quad (6.7)$$

Interpretation of p -value and z -value

The p -value gives a measure of the significance and is directly related to the statistical significance z -value with

$$p\text{-value} = \int_{z\text{-value}}^{\infty} \frac{1}{\sqrt{2\pi}e^{-x^2/2}} dx. \quad (6.8)$$

The error function

$$\operatorname{erf}(x) = \int_0^x \frac{2}{\sqrt{\pi}} e^{-t^2} dt = \frac{2}{\sqrt{\pi}} \sum_{n=0}^{\infty} \frac{(-1)^n x^{2n+1}}{(2n+1)n!} \quad (6.9)$$

is a s-shaped curve probability integral called sigmoid function with the argument x and used to calculate the z -value. The inverse error function is calculated numerically¹. Transforming, the error function in the p -value integral for $p\text{-value} \leq 0.5$ results in

$$z\text{-value} = \sqrt{2} \cdot \operatorname{erf}^{-1}(1 - 2 \cdot p\text{-value}) \quad (6.10)$$

for the significance. The relationship for all p -values is depicted in Fig. 6.1. The significance gets negative for $p\text{-value} > 0.5$ so that the relation does not work anymore. Therefore, only $p\text{-value} < 0.5$ is considered in the following hypothesis tests. The $p\text{-value} > 0.5$ can be neglected since the corresponding significance is $z\text{-value} = 0$.

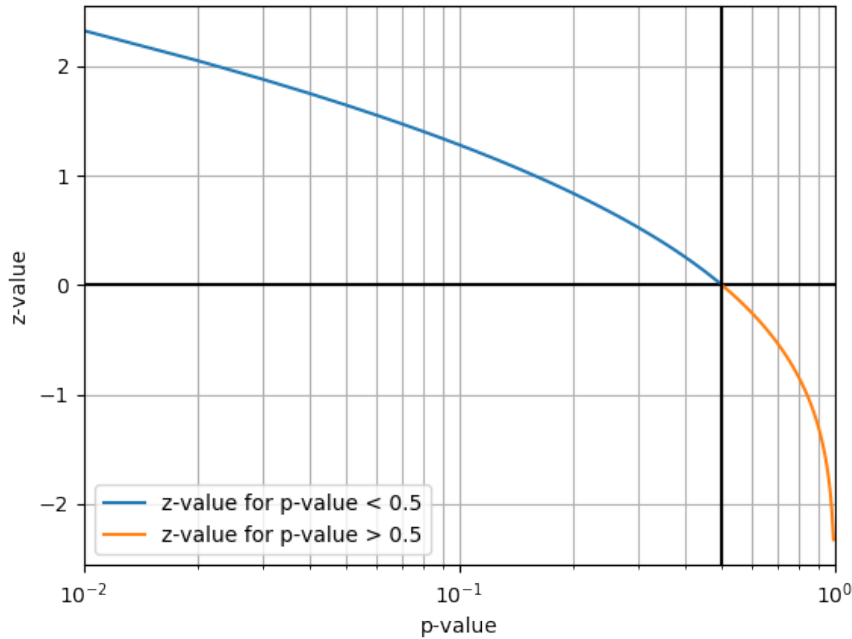


Figure 6.1: Relationship between significance and p -value is given by $z\text{-value} = \sqrt{2} \cdot \operatorname{erf}^{-1}(1 - 2 \cdot p\text{-value})$. For $p\text{-value} > 0.5$, the significance would get negative as highlighted in orange.

The significance level measures the magnitude of deviations between the results and the model. For an excess, the significance is defined positive and for a deficit negative. In

¹Programming languages do usually have a defined function to calculate it. For `R` it is `TMath::ErfInverse(x)` and for `Python` one can use `scipy.special.erfinv(x)`.

Table 6.1: Interpretations of p -value and z -value adapted from Ref. [5].

z -value	≥ 0	< 0	5	1
p -value	≤ 0.5	> 0.5	$2.87 \cdot 10^{-7}$	0.15
	deviations	no deviations	discovery threshold	1-sigma statistical fluctuation

physics, an evidence is given for a deviation of z -value ≥ 3 . A new discovery can be proclaimed if the deviation is significant with z -value ≥ 5 . Further interpretations are shown in Table 6.1.

6.2.2 Bin-by-bin hypothesis testing

In the bin-by-bin hypothesis test, the number of measured events D is compared to the number of expected events H_0 for each bin individually. The z -value is calculated for every bin.

The z -value can be directly calculated by [5]

$$z\text{-value} = \frac{x - \mu}{\sigma} \quad (6.11)$$

for a Gaussian distribution with a known mean value μ and a standard deviation σ .

As described in Section 6.1, for a data set used in this project, a Poisson distribution can be assumed. For bins which follow a Poisson distribution, the z -value is determined through the p -value.

For a Poisson distribution, the p -value is given by [5]

$$p\text{-value} = \begin{cases} \sum_{n=D}^{\infty} \frac{B^n}{n!} e^{-B} = 1 - \sum_{n=0}^{D-1} \frac{B^n}{n!} e^{-B} & \text{for } D > B \\ \sum_{n=0}^D \frac{B^n}{n!} e^{-B} & \text{for } D \leq B \end{cases} \quad (6.12)$$

with the observed number of events D and the expected background B . This is the case-by-case analysis for an excess $D > B$ and a deficit $D \leq B$. For $D \leq B$, the summation goes from 0 to D to include all possible values of a deficit whereas for $D > B$, the summation goes until infinity to include all possible excesses.

The Gamma function is used to calculate the p -value directly for a Poisson distribution. The Gamma function for integer arguments is the factorial function with the argument minus one

$$\Gamma(n) = (n - 1)! .$$

The incomplete Gamma function is given by

$$\Gamma(D, B) = \int_B^{\infty} t^{D-1} e^{-t} dt \quad (6.13)$$

and this gives the upper regularized Gamma function²

$$Q(D, B) = \frac{\Gamma(D, B)}{\Gamma(D)} \quad (6.14)$$

²The Python function is `scipy.special.gammainc` and for ROOT one can use `ROOT::Math::inc_gamma_c(z,x)`.

with which the p -value is calculated according to

$$p\text{-value} = \begin{cases} 1 - \frac{\Gamma(D,B)}{\Gamma(D)} = 1 - Q(D, B) & \text{for } D > B \\ \frac{\Gamma(D+1,B)}{\Gamma(D+1)} = Q(D+1, B) & \text{for } D \leq B. \end{cases} \quad (6.15)$$

This is a way to simplify the calculation of the p -value.

6.2.3 Hypothesis hyper test

A hypothesis test becomes a hyper test, if it is executed several times for various positions of the spectrum in the data set and then the results of each hypothesis test is compared and concluded to one result.

Assuming a binned data set with plenty of bins. Then it is statistical natural that one bin fluctuates significantly from the hypothesis H_0 even if there should be no significant deviation. This is called “Look-elsewhere effect” and it is taken into account in a hypothesis hyper test. Such single-bin fluctuations are excluded by considering all bins on the same basis. This means that the probability to find such or a higher deviation anywhere in the spectrum by chance is taken into account.

A hyper test includes N hypothesis tests. Every single hypothesis test works as described in Section 6.2.1 and is performed on the data D and the pseudo data. Every hypothesis test determines a p -value so that N p -values are calculated for one data set. The smallest p -value is picked and defines the “hyper test test statistic” t . It follows the principle the smaller the p -value the higher is the test statistic. An arbitrary strictly monotonic decreasing function can be chosen like

$$t = -\log(\min\{p\text{-value}\}) \quad (6.16)$$

for the definition of the hyper test test statistic. Examples for hypothesis hyper tests are the BumpHunter and the TailHunter algorithm.

7 Statistical Analysis and Implementation

This chapter sets a focus on the methods to determine the difference between the measured data and the background prediction. Two types of analysis will now be explained: Several bin-by-bin comparison techniques [5] and global comparisons in the form of two hypothesis hyper tests (BumpHunter and TailHunter algorithm) [6]. Then, the methods are applied and implemented in the Jupyter notebook. Code examples are shown. The subsequent discussion compares the results of the different techniques. Finally, a proof-of-principle with the published results of the ATLAS collaboration is performed.

There are several methods to depict the differences between a data set D and the background prediction B . The aim of such a graph is to give the reader an impression of how well the measured data fit to the background model or the theory. It should show, at which points an excess or a deficit in the data is observed. Furthermore, in particle physics it is interesting to see the magnitude of the deviations from the background expectation for the respective data points.

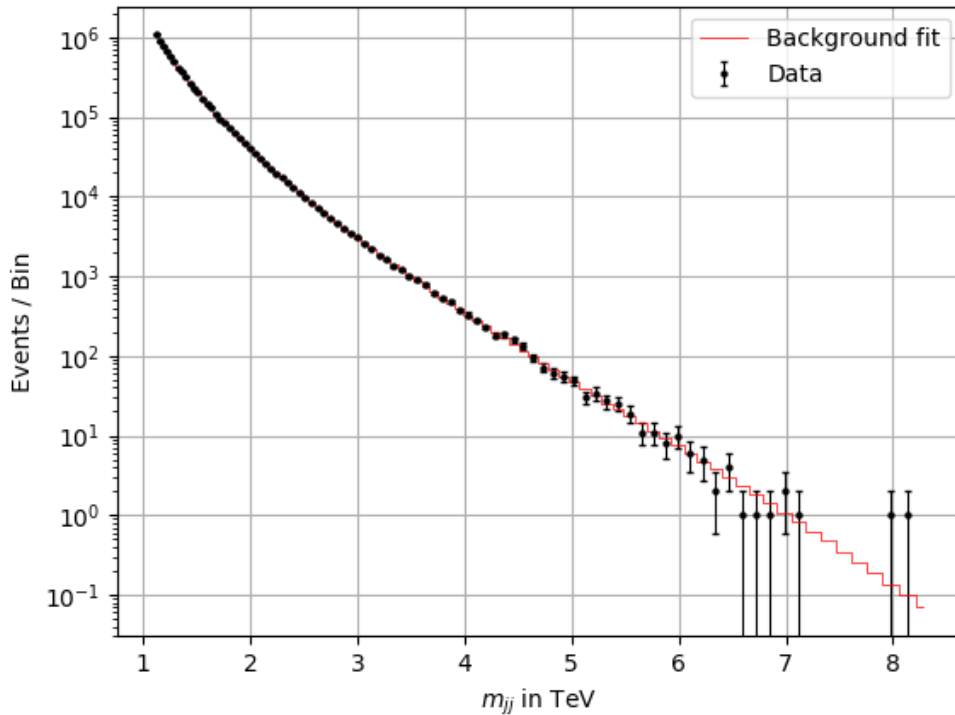


Figure 7.1: The measured data and its expectation from Table 1 in Ref. [3] are shown in one graph. The expectation is labeled as background in red and is determined by a four-parameter fit function described in Section 5.4. The data is illustrated as black data points. The uncertainties are given by the statistical uncertainty of \sqrt{N} with number of events N for the data points. The background uncertainties are negligible (see Section 5.4) and hence not shown.

An overview is given when the number of events per bin and the values of the background model are depicted against the binned x-parameter, here m_{jj} . Deviations for single points can be seen and a rough statement regarding the agreement can be made. The significance of those deviations cannot be seen. For a logarithmic scale, it is harder to interpret the

absolute differences. Fig. 7.1 shows the data and the predicted background events as a function of m_{jj} using a log scale.

7.1 Bin-by-Bin Techniques

The data taken is counted in bins of varying width. To prepare the histograms for the comparison, first, the bin-widths are calculated in the Jupyter notebook. The left edge `widthlow`, the right edge `widthhigh` and the bin center `x` are given in Table 1 in [3] in the second, third and first column, respectively. For each bin i , the bin width `width` is calculated by

$$\text{width}[i] = \text{widthhigh}[i] - \text{widthlow}[i]. \quad (7.1)$$

```
# Calculate the width of each bin
width=[]
i=0
# Calculate the width for all entries
while i < len(widthlow):
    # The width is the difference of the high and the low edge
    width.append(widthhigh[i]-widthlow[i])
    i=i+1
```

7.1.1 Absolute and Relative Difference

The first method to investigate the differences between data and background model is to take the absolute difference ΔE in the list `absolute`

$$\Delta E = D - B \Rightarrow \text{absolute}[i] = y[i] - yb[i] \quad (7.2)$$

at each bin i . The number of events in the data set is $y=D$ and in the background prediction it is $yb=B$. An excess has a positive and a deficit a negative value. This depicting technique is applied in Fig. 7.2.

```
# Determine the values of the absolute difference
absolute=[]
i=0
# Calculate the abs. difference for all bins
while i < len(x):
    # Subtract the background from the measured data value
    absolute.append(y[i]-yb[i])
    i=i+1
```

The absolute difference is usually high for high populated bins and low for bins of very low population. This method does not give any useful information about how the data set is in accordance with the background model. It does not show any significant deviations for data counts, which span over several orders of magnitude.

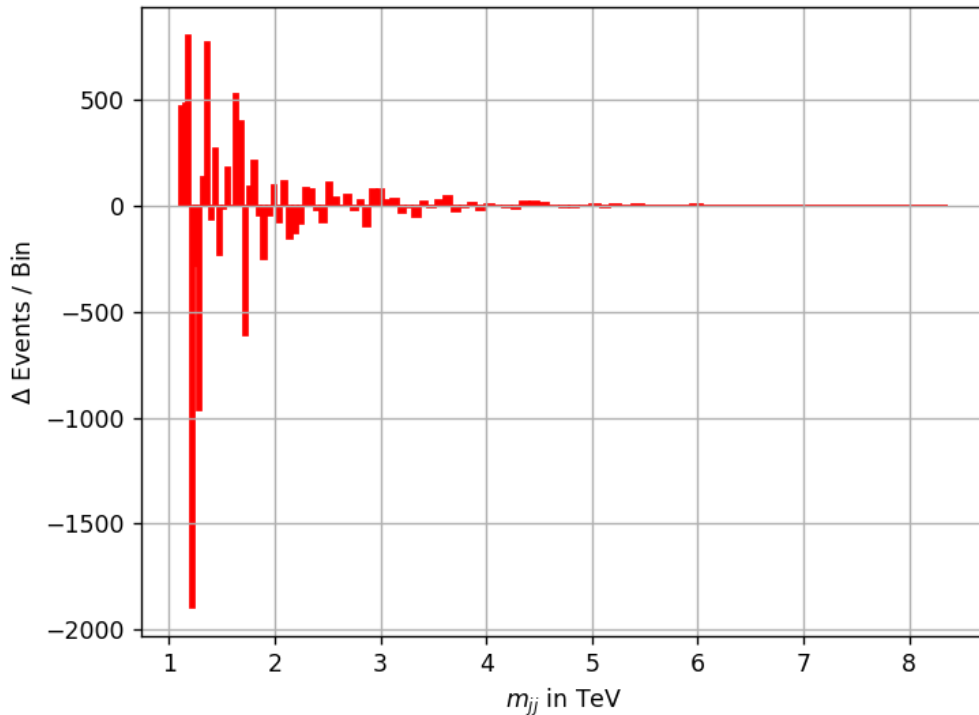


Figure 7.2: The absolute difference between data and background is shown in red for each bin. For high-populated bins, the difference is high and for low-populated bins almost zero.

One other intuitive way to investigate the deviations of data and expectations is to calculate the ratio of data to background

$$\frac{\text{Data}}{\text{Expected}} = \frac{D}{B} \quad (7.3)$$

Then, the relative difference is given by

$$\frac{D}{B} - 1 = \frac{D - B}{B} \Rightarrow \text{rel}[i] = (y[i] - y_b[i]) / y_b[i] \quad (7.4)$$

in each bin i . An excess of data results in a positive relative difference and a deficit in a negative value. The relative difference for the m_{jj} distribution is shown in Fig. 7.3.

```
# Calculation of the relative difference for all bins
rel = []
i=0
while i < len(y):
    # Adding the rel. difference of each bin to the list 'rel'
    rel.append((y[i]-yb[i])/yb[i])
    i=i+1
```

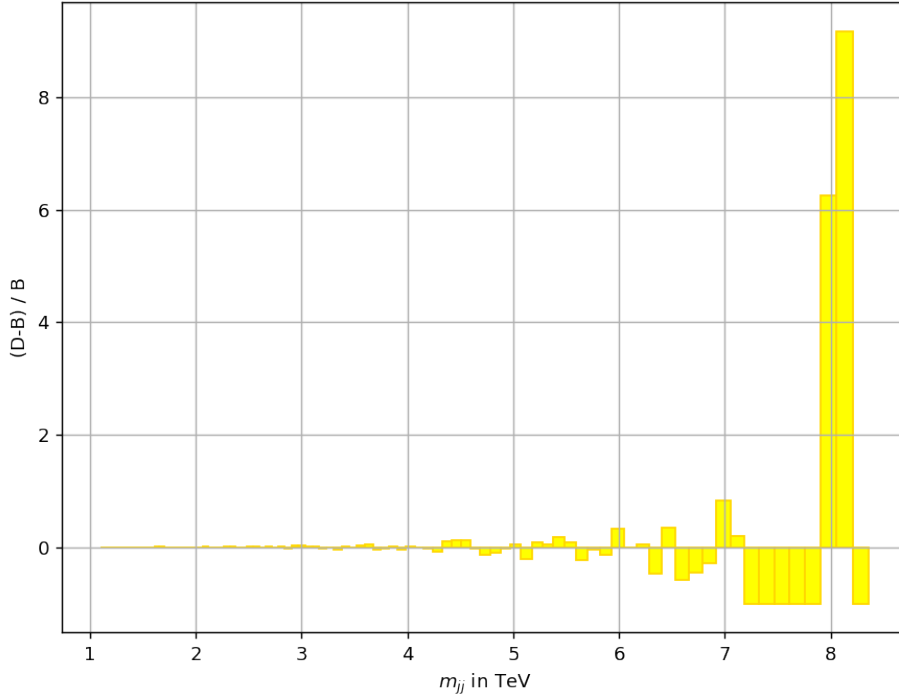


Figure 7.3: The relative difference between the data and background is shown in yellow for each bin. By comparing the relative difference with the population of the bins in Fig. 7.1, it becomes clear that for high populated bins, the relative difference is almost zero. For high invariant dijet masses m_{jj} deviations appear in low-populated bins.

The relative difference for low values of m_{jj} is almost zero. For $m_{jj} > 4$ TeV, the absolute value of the relative difference rises. Deviations in form of an excess as well as a deficit appear. The highest relative difference is present at $m_{jj} = 8$ TeV for two adjacent bins with an excess of over 600% and 800%.

This way of plotting does not show the significance. For high -populated bins, significant discrepancies can be hidden since the relative difference becomes smaller for a large background. The fluctuations of the relative difference rise for low-populated bins. It seems that most fluctuations are observed at the low-populated bins. This is the deficit of the method and has a meaningful impact if the data set spans over several orders of magnitude. It does not statistically quantify the agreement between data and background prediction.

7.1.2 Gaussian approximation of the significance

The Poisson distribution approximates the Gaussian distribution for high number of events as presented in Section 6.1. As shown for a Poisson distribution (c.f. Eq. (6.4)), the standard deviation is $\sigma = \sqrt{\mu}$. Using Eq. (6.11), the statistical significance z -value can be approximated by

$$z\text{-value} = \frac{x - \mu}{\sigma} = \frac{x - \mu}{\sqrt{\mu}}. \quad (7.5)$$

Applying this to the example with the measured data D and the estimated background B , the significance z can be approximated by

$$z\text{-value} = \frac{D - B}{\sqrt{B}}. \quad (7.6)$$

$$\Rightarrow \text{app}[i] = (y[i] - yb[i]) / (yb[i]**(0.5))$$

for each bin i . The results of the approximation are presented in Fig. 7.4. The highest deviation can be seen for $m_{jj} \approx 8$ TeV with almost 3 standard deviations. For all other bins, the deviation is below two standard deviations.

```

# Calculate the Gaussian approximation of the significance
# List for the values of the approximation
app=[]
i=0
while i < len(y):
    # Calculation and adding the values to the list
    app.append((y[i]-yb[i])/(yb[i]**(0.5)))
    i=i+1

```

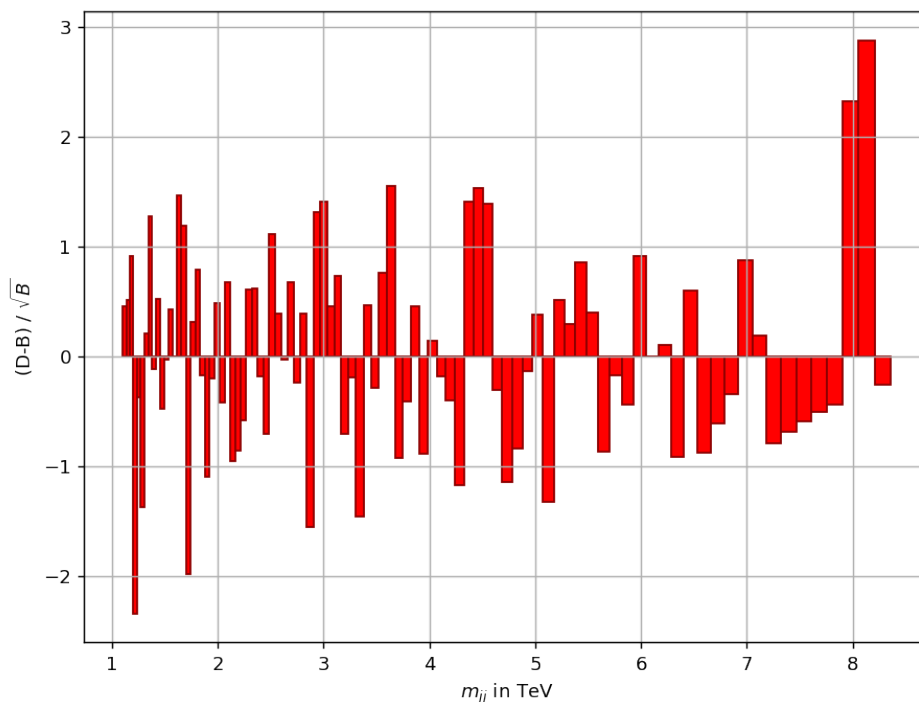


Figure 7.4: The significance is approximated by $\frac{D-B}{\sqrt{B}}$. An excess of data is given by a positive and a deficit by a negative value. The most significant bins are observed at $m_{jj} \approx 8$ TeV at low-populated bins.

In the Jupyter notebook, there is a short code applied which separates the bins with an excess (plus) to the bins with a deficit (minus). Thereby, the two types of deviations can

be depicted in different colors which makes the plot clearly arranged as shown in Fig. 7.5.

```

# All deficits are added to the list called 'minus'
minus=[]
i=0
while i < len(y):
    if app[i]<0:
        minus.append(app[i])# Add all neg. values to the list
    else:
        minus.append(0) # Positive values are set to zero to
                        # keep the positions in the list
    i=i+1
# All excesses are added to the list 'plus'
plus=[]
i=0
while i < len(y):
    if app[i]>0:
        plus.append(app[i])
    else:
        plus.append(0)
i=i+1

```

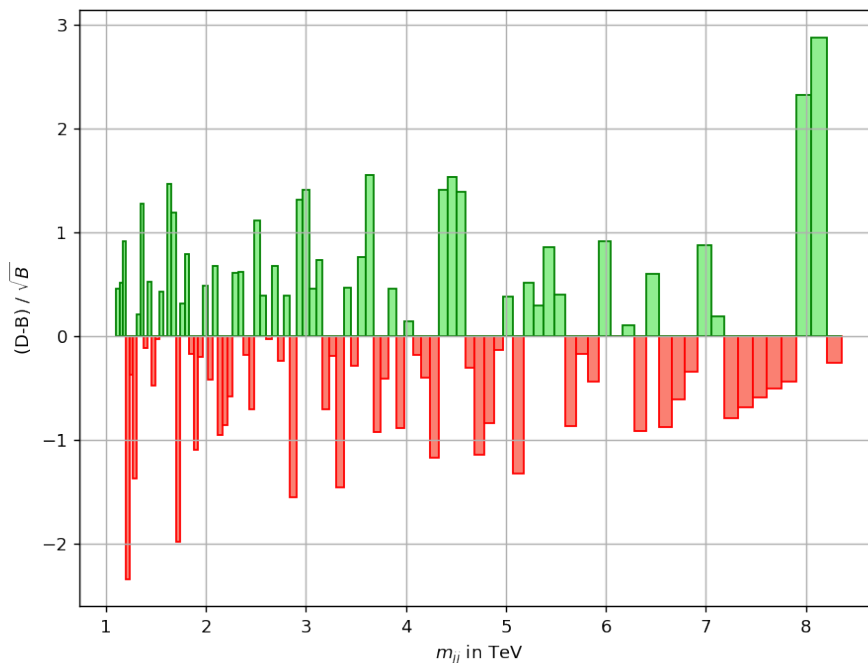


Figure 7.5: The plot of Fig. 7.4 is repeated with different colors for excesses and deficits.

Since the Poisson distribution approximates the Gaussian distribution for high-populated bins, this way of plotting is valid for a large background B . However, it fails for bins with only a few entries. No reliable statement about the significance can be made for bins

with less than 10 entries. According to Tab.1 in [3], for bins from $m_{jj} > 5.874$ TeV the approximation is not valid anymore. For data sets with only high-populated bins in the interesting range of the observable, this way is easy and efficient to use.

7.1.3 The Significance

The significance is calculated as described in Section 6.1 via the p -value. The p -value is determined with Eq. (6.12). The Python package `scipy` has a function for the incomplete gamma function called `scipy.special.gammainc(D, B)` which is used here, to calculate the p -value. The significance (c.f. Eq. (6.15)) is then determined using the `scipy` function for the inverse error function `scipy.special.erfinv`. Two cases are considered: For an excess with $D > B$, the significance is chosen to be positive and for a deficit with $D < B$, the significance is chosen to be negative.

```

# Function for calculation of the Poisson p-value
# with the incomplete gamma function
def pvalue(D,B):
    if D>B :                               # For an excess
        p = scipy.special.gammainc(D, B)
    else :                                   # For a deficit
        p= 1-scipy.special.gammainc(D+1, B)
    return p

# Function for calculation of the significance (z-value)
# with the inverse errorfunction
def zvalue(p):
    if y[i]>yb[i]:                           # For an excess
        z=2**(1./2)*scipy.special.erfinv(1-2.*p)
    else:                                     # For a deficit
        z= -2**(1./2)*scipy.special.erfinv(1-2.*p)
    return z

```

The significance `sig` in each bin `i` is calculated as

$$\text{sig}[i] = \text{zvalue}(\text{pvalue}(y[i], yb[i])).$$

```

sig=[]                                     # List for significance
i=0
# Calculate the zvalue in dependence of the pvalue of
# y and yb and add it to the list
while i < len(y):
    sig.append(zvalue(pvalue(y[i], yb[i])))
    i=i+1

```

The results are presented in Fig. 7.6 showing deviations up to 2.4 standard deviations. For some bins between $m_{jj} = 7$ -8 TeV, a positive significance is shown even if a deficit is observed.

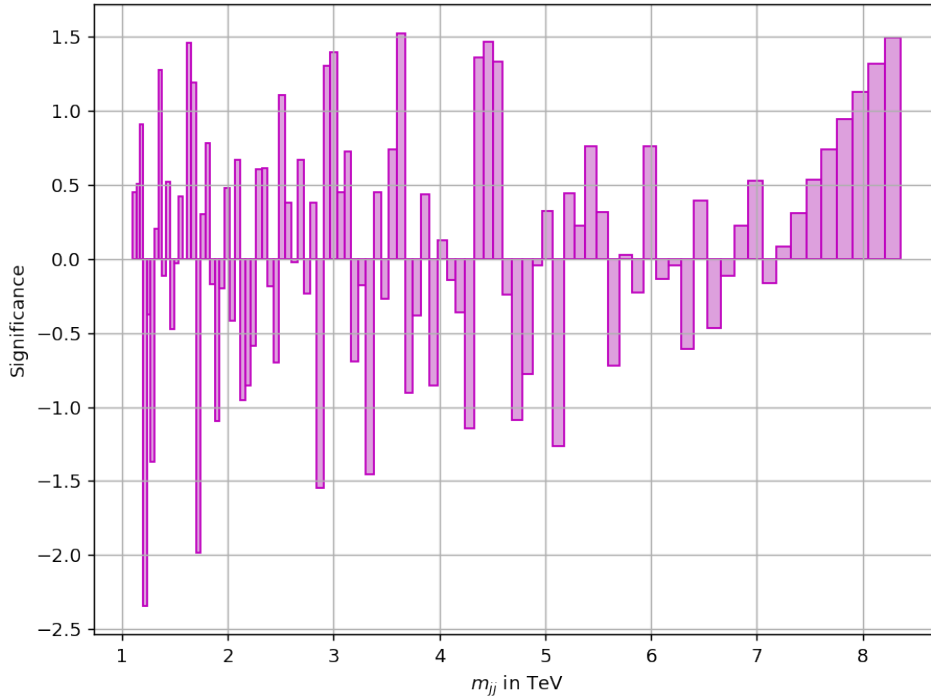


Figure 7.6: The deviations are shown in form of the significance. The significance is calculated via the Poisson p -value.

The p -value is directly transferred into the significance with Eq. (6.10) and therefore is so to speak already a significance. As presented in Table 6.1, the significance is zero or negative if the p -value is greater or equal $p\text{-value} \geq 0.5$. Therefore, in the next step, the bins with a $p\text{-value} > 0.5$ are excluded. This restriction is performed in Fig. 7.7.

```

# Perform the cut pvalue < 0.5 and determine all pvalue < 0.5
sigp=[]
i=0
while i < len(y):
    if pvalue(y[i], yb[i])<0.5:                # For pvalue < 0.5
        # ...add the pvalue
        sigp.append(zvalue(pvalue(y[i], yb[i])))
        i=i+1
    else:                                       # For pvalue > 0.5
        sigp.append(0)                          # ...add pvalue=0
        i=i+1

```

Fig. 7.6 and Fig. 7.7 show the significance for each bin. While in Fig. 7.6 the z -value was calculated for all bins, in Fig. 7.7 only relevant bins with $p\text{-value} \leq 0.5$ are presented. For $p\text{-value} > 0.5$, the significance z -value would become negative due to the trend of the inverse error function. The significance is then set to zero for $p\text{-value} \geq 0.5$ as presented in Fig. 7.7.

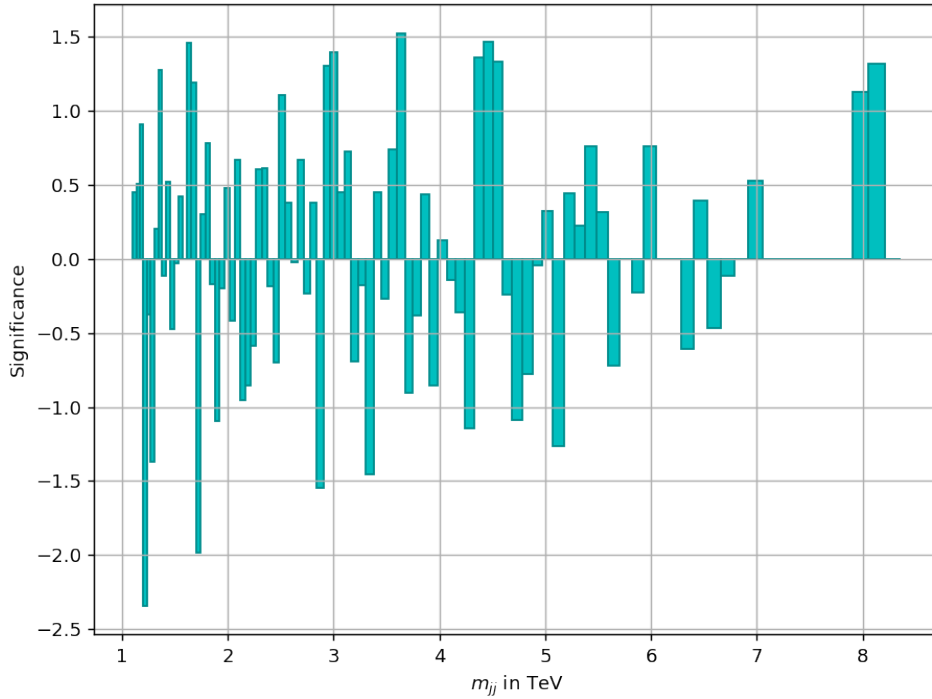


Figure 7.7: The significance is plotted and the p -value cut with p -value > 0.5 is applied. Only bins with p -value < 0.5 are shown.

Depicting the significance is the most reliable way to investigate the differences between data and the background model. The calculation of the significance with the p -value from the Poisson distribution gives the accurate value of the significance.

The deviations of the data set from the background model are between approximately $+1.5$ and -2.4 standard deviations. Evidence is accepted for 3 standard deviations and a discovery is proclaimed for a significance higher than 5 standard deviations. Considering the bin-by-bin analysis, no significant excess or deficit is observed.

7.2 Comparison of the Bin-by-Bin Analyze

The differences between the Gaussian approximation of the significance and the significance are recapped in Fig. 7.8. The absolute and relative difference cannot directly be compared with those methods since the unit is not in standard deviations.

For large bin populations, the absolute difference is very high and drops down to nearly zero for the low-populated bins. The relative difference shows a reversed behaviour. Highly populated bins have a relative difference of almost zero and the relative difference increases rapidly for low populated bins. By comparing those characteristics with the results of the other techniques, it becomes clear that both methods cannot be used for reliably quantifying excesses or deficits.

Fig. 7.8 confirms that the approximation of the significance $\frac{D-B}{\sqrt{B}}$ is a quite good approximation for large populated bins, here in the range of $1 \text{ TeV} - 5.874 \text{ TeV}$. For lower populations in the bins and here subsequently for higher invariant dijet masses m_{jj} , the

approximation breaks down. For p -value >0.5 , the significance formula also breaks down and would give a significance in the wrong direction. Thus, Fig. 7.7 gives the most reliable result for the significance in the bin-by-bin analysis.

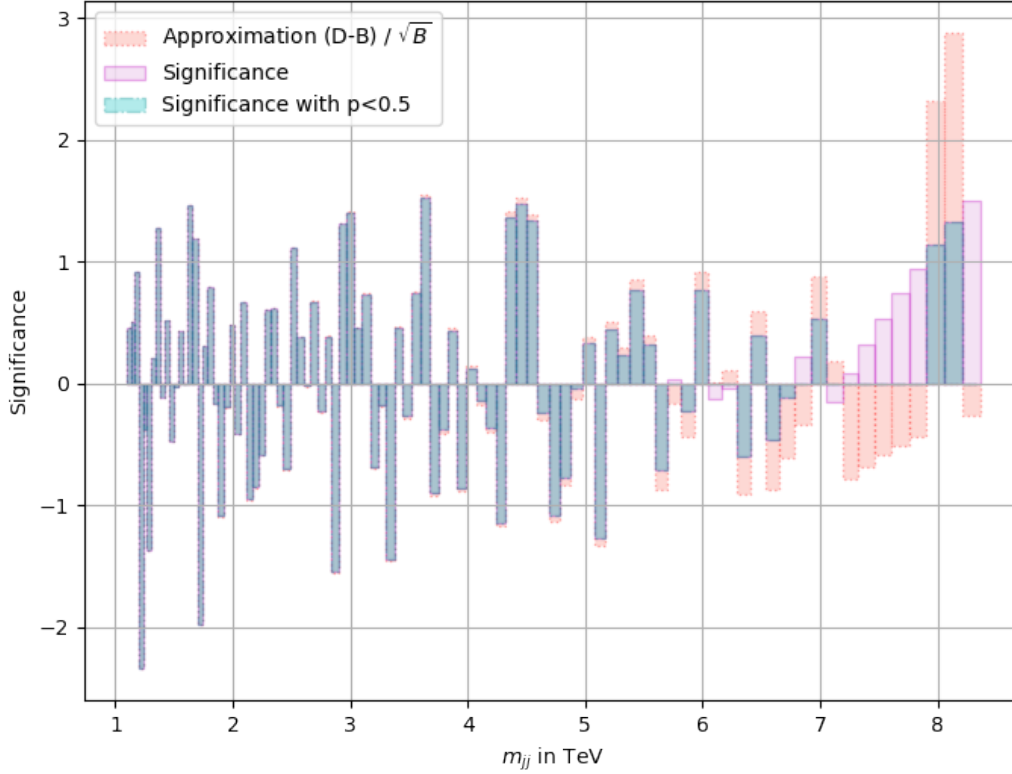


Figure 7.8: Three ways of quantifying excesses and deficits are shown. The approximation of the significance in red agrees with the significance for low m_{jj} and deviate from it for higher m_{jj} . The turquoise and purple way of depicting the significance differ only in low populated bins for high m_{jj} .

7.3 BumpHunter and TailHunter algorithm as a global comparison technique

The BumpHunter and the TailHunter algorithm are hypothesis hyper tests that follow the structure of a hypothesis test described in Section 6.2.1. The Bumphunter algorithm is a hyper test that finds the most deviant excess in a data set compared to the background prediction as the hypothesis. The TailHunter is an easy generalization of the bumphunter concept. Instead of looking for bumps anywhere in the spectrum, the TailHunter ‘hunts’ for tails. That means that a continuous excess of data at the tail of the spectrum would be observed by the tailhunter. The tail of a spectrum is defined as the falling down curve on the right edge.

Both algorithms are implemented in the Jupyter notebook based on the code of Peter Wallis in Ref. [100]. In this implementation, the “Look-elsewhere-effect” is taken into account. It considers the probability to find an excess or a higher excess than the observed one anywhere in the spectrum [101]. The principle of operation and the results are

presented and discussed in this subchapter.

7.3.1 The Bumhunter algorithm

The hypothesis test is performed several times on the data set looking at different positions and for different widths. First, the positions and widths of the windows are defined. Then, the performance of the hypothesis test is described. The coding parts of the algorithm are implemented.

Positions and widths of the central window W_c The central window W_c is the area in the spectrum where the bumhunter operates. For the data in Tab.1 in Ref. [3], the width of the central window is chosen to be minimum 1 bin and to be maximum $\lfloor \frac{N}{2} \rfloor$ bins with the number N of non-zero background bins in the spectrum. For all window sizes in the range of $(1, \lfloor \frac{N}{2} \rfloor)$ bins, the positions are shifted in the spectrum from the lowest to the highest observed x-value (here invariant dijet mass) by a number of bins with the stepsize

$$\text{step size} = \max \left\{ 1, \left\lfloor \frac{W_c}{2} \right\rfloor \right\}.$$

This ensures, that candidates for excesses remain in overlapping windows and no windows with significant excesses are skipped. On the other hand it reduces the computational time compared to the procedure where all possible windows are checked with step size= 1. The hypothesis test is applied to all variations of window widths and positions described above.

```
def all_windows():
    # Set width of the central Window Wc
    min_win_size = 1
    max_win_size = math.floor((search_hi - search_lo)/2)
    for binwidth in range(min_win_size, max_win_size):
        # Set max step size
        step = max(1, math.floor(binwidth / 2))
        for pos in range(search_lo, search_hi - binwidth, step):
            yield pos, pos + binwidth
```

Sidebands To ensure that the window of an observed bump is not in a not well modelled region, sidebands are included. A sideband is defined as the region left or right to the central window W_c with a width of

$$\text{sideband width} = \max \left\{ 1, \left\lfloor \frac{W_c}{2} \right\rfloor \right\}.$$

The left (L) and right (R) sidebands are investigated by calculation of the Poisson p -value \mathcal{P} with Eq. (6.12). The data $d_{L,R}$ and the background $b_{L,R}$ are counted and \mathcal{P} is calculated with the sum of data and background points in the sideband. If any of the two sidebands have a resulting p -value of

$$\mathcal{P}(d_{L,R}, b_{L,R}) \leq 10^{-3}$$

the p -value is set to one for the central window since it is in a not well modelled region. However, the sideband criteria with $\leq 10^{-3}$ is arbitrarily chosen corresponding to a 3σ

deviation in the sideband.

```

def all_leftsidebands():
    # Set width of the central Window Wc
    min_win_size = 1
    max_win_size = math.floor((search_hi - search_lo)/2)
    for binwidth in range(min_win_size, max_win_size):
        # Set width of the sideband
        side_size = max(1, math.floor(binwidth / 2))
        # Set max step size
        step = max(1, math.floor(binwidth / 2))
        for pos in range(search_lo, search_hi - binwidth, step):
            yield pos - side_size, pos

def all_rightsidebands():
    # Set width of the central Window Wc
    min_win_size = 1
    max_win_size = math.floor((search_hi - search_lo)/2)
    for binwidth in range(min_win_size, max_win_size):
        # Set width of the sideband
        side_size = max(1, math.floor(binwidth / 2))
        # Set max step size
        step = max(1, math.floor(binwidth / 2))
        for pos in range(search_lo, search_hi - binwidth, step):
            yield pos + binwidth, pos + binwidth + side_size

```

Definition of the test statistic t_0 and p -value To investigate the central window W_c , data d_c and background b_c is counted and their sum over the bins in the central window is taken. d_c is an integer number and b_c in is real number.

In this implementation of the BumpHunter, a method is chosen which calculates the p -value in a window directly without determining the test statistic t . This is possible, since the p -value is calculated for all windows equally and it is only of interest which window has the smallest p -value. The p -value is calculated as the Poisson p -value described in Eq. (6.12)

$$p\text{-value} = \begin{cases} \sum_{n=d_c}^{\infty} \frac{b_c^n}{n!} e^{-b_c} = 1 - \sum_{n=0}^{d_c-1} \frac{b_c^n}{n!} e^{-b_c} & \text{for } d_c > b_c \\ \sum_{n=0}^{d_c} \frac{B^n}{n!} e^{-b_c} & \text{for } d_c \leq b_c \end{cases}$$

with d_c and b_c , respectively. In the implementation, the same functions are used as in Section 7.1.3. Windows with a deficit, namely $d_c \leq b_c$, are ignored in the further investigation since only bumps/excesses are of interest. Furthermore, windows in a discrepant region are excluded. Both are done by setting the p -value to 1. The calculated p -value for each window is illustrated in Fig. 7.9. This lowest p -value is roughly between 4.3 TeV and 4.6 TeV. The window with the lowest p -value is chosen for the further algorithm.

```

def pvalueside(lo, hi):

```

```

#sum all values for data and background
d = data[lo:hi].sum()
b = bkg[lo:hi].sum()
if b == 0:
    assert d == 0
    return 1 #Special case
if d < b:
    return 1 # Deficits
if d > b:
    p = scipy.special.gammainc(d, b)
    return p # Excesses

```

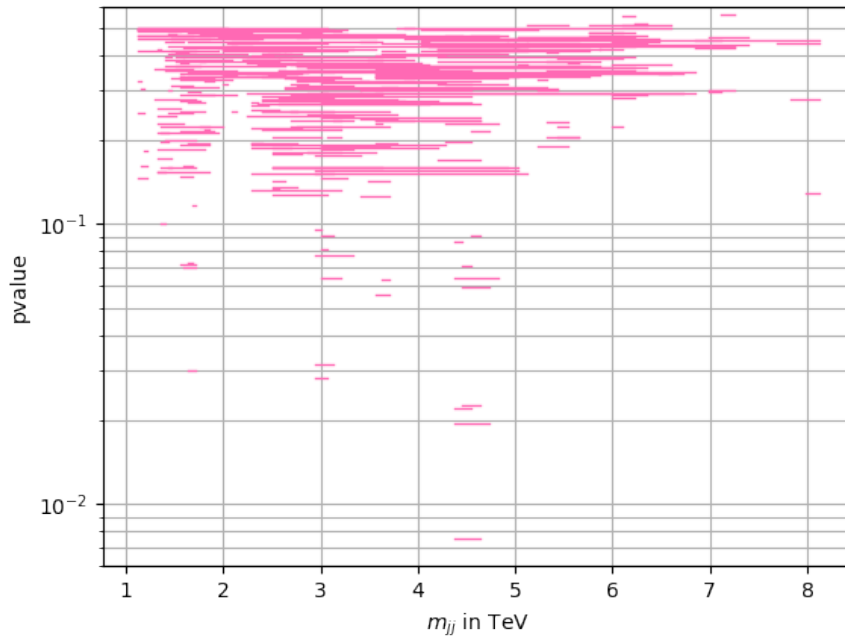


Figure 7.9: All considered windows in the BumpHunter algorithm with p -value < 0.6 are shown. The level of the window is the corresponding Poisson p -value. To distinguish the windows in interesting areas (low p -value), a logarithmic scale is chosen.

The BumpHunter test statistic t_0 is defined for the lowest p -value in Eq. (6.16) and given by

$$t_0 = -\log(p\text{-value}_{\min})$$

between data d_c and background b_c . For a decreasing p -value, the test statistic t increases which means a higher difference between data and expectation.

Now, the important part follows: How significant is the excess in the window with the test statistic t_0 ? In order to investigate this, a new kind of p -value is introduced which hereafter will be called ‘BumpHunter p -value’. For a small BumpHunter p -value, the probability is small that the hypothesis H_0 is wrongly ruled out and therefore, a small BumpHunter p -value gives a more significant excess. A high BumpHunter p -value would mean that no significant bump is observed. Since the BumpHunter p -value is a probability it ranges from 0 to 1.

Determination of the BumpHunter p -value The BumpHunter p -value is estimated using pseudo experiments. Pseudo data is created following the expectation of H_0 using the function `numpy.random.mtrand.poisson`. In total, 10000 pseudo data sets are created. For each pseudo data set, a test statistic t is calculated in the same way as for t_0 for the measured data set. Here, the look-elsewhere³, read Ref. [102]) effect is taken into account by taking the window with the lowest p -value in each pseudo experiment.

```
#Make pseudo data under a special prediction
import numpy as np
def make_toys(prediction, n):
    return np.random.mtrand.poisson(prediction,
                                     size=(n, len(prediction)))
```

A distribution of 10000 test statistics t is created and compared to t_0 as in Fig. 7.10. Since the test statistic distribution t is not continuous, Eq. (6.7) is used to calculate the p -value. In the Python program, the number of pseudo experiments with $t_0 > t$ is counted with the function `scipy.stats.percentileofscore` and gives the percentage of t 's below t . The p -value is then calculated by

$$p\text{-value} = 1 - (\text{percentileofscore}(t, t_0)/100) \quad (7.7)$$

since it is defined as $P(t \geq t_0|H_0)$.

```
pvalue = 1. - (scipy.stats.percentileofscore(pseudo_experiments,
                                             measurement) / 100.)
```

Results of the BumpHunter For the data in Table 1 in Ref. [3], the test statistic is

$$t_0 \approx 4.8841$$

with a window in between the bins with the number 58 and 61 which is in the range of $m_{jj} = 4.326 - 4.595$ TeV. A BumpHunter p -value of around

$$p\text{-value} \approx 0.69$$

was calculated. Hence, no significant excess anywhere in the spectrum is observed.

7.3.2 Generalization of the BumpHunter: TailHunter

The TailHunter is an easy generalization of the BumpHunter concept. Instead of looking for bumps anywhere in the spectrum, the tail hunter 'hunts' for tails. That means that a continuous excess of data at the tail of the spectrum can be detected by the tail-hunter. The tail of a spectrum is defined as the falling right edge. Since the TailHunter is a generalization of the BumpHunter, the principle of operation is the same as for the BumpHunter. However, some criteria are chosen differently:

³The calculation of the significance must take into account that such an excess could occur anywhere in the range without being a signal. The look-elsewhere effect takes into account how large the probability is to find such or a more extreme bump anywhere in the range. This is defined via a the trial factor which is the ratio between the probability to observe the excess at a fixed point and anywhere in the range.

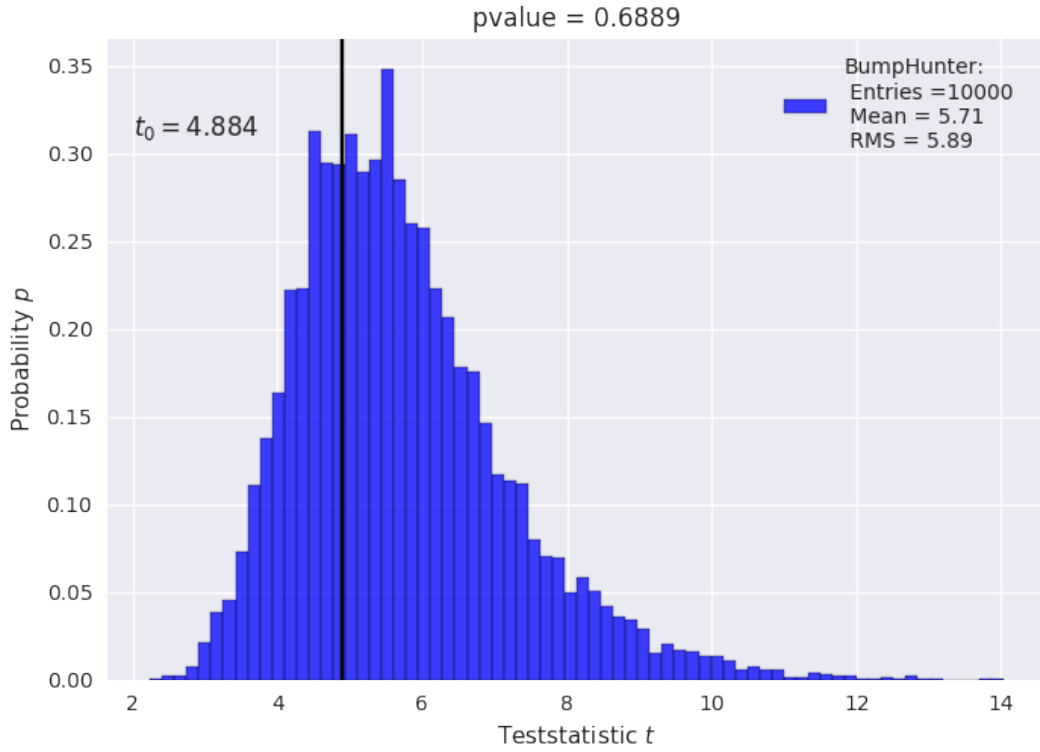


Figure 7.10: Distribution of the BumpHunter test statistic t . The observed test statistic is $t_0 = 4.884$. The p -value is determined after performing 10000 pseudo experiments as 0.6889.

- No sideband criteria are chosen.
- The windows are so chosen that the last bin with data is always the right edge of the window.
- The windows size is compressed by steps of one bin.

The Poisson p -value and the test statistic t_0 for the smallest Poisson p -value is calculated in the same way as for the BumpHunter. The Poisson p -value distribution for the corresponding windows is shown in Fig. 7.11. Also, pseudo data are created to determine the TailHunter p -value. The comparison between the test statistic t_0 and the test statistics of the pseudo experiments t is shown Fig. 7.12.

Results of the TailHunter For the data in Table 1 in Ref. [3], the test statistic is

$$t_0 \approx 3.7354$$

with a window in between the bins with the number 89 and 91 which is in the range of $m_{jj} = 7.904 - 8.364$ TeV. A BumpHunter p -value of around

$$p\text{-value} \approx 0.24$$

was calculated. No significant excess in the tail is observed.

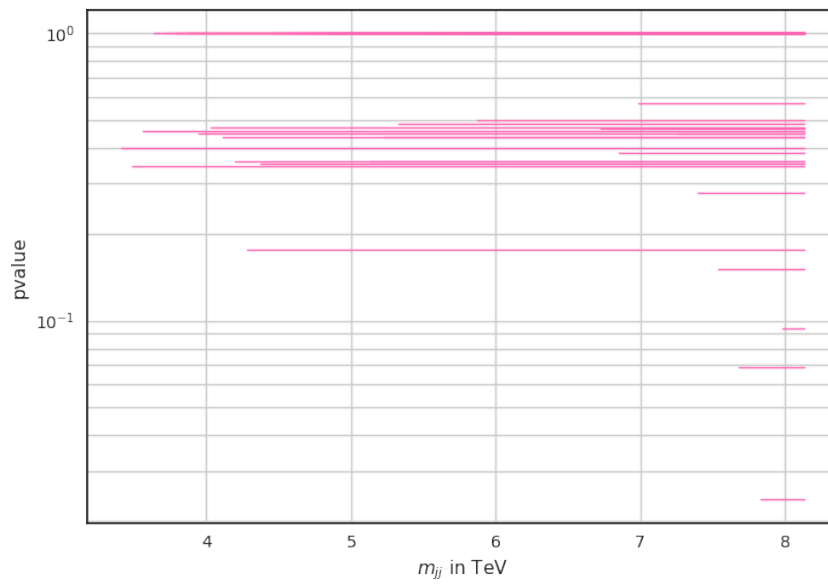


Figure 7.11: All considered windows in the TailHunter algorithm are shown. The level of the window is the corresponding Poisson p -value. To distinguish the windows in interesting areas (low p -value), a logarithmic scale is chosen.

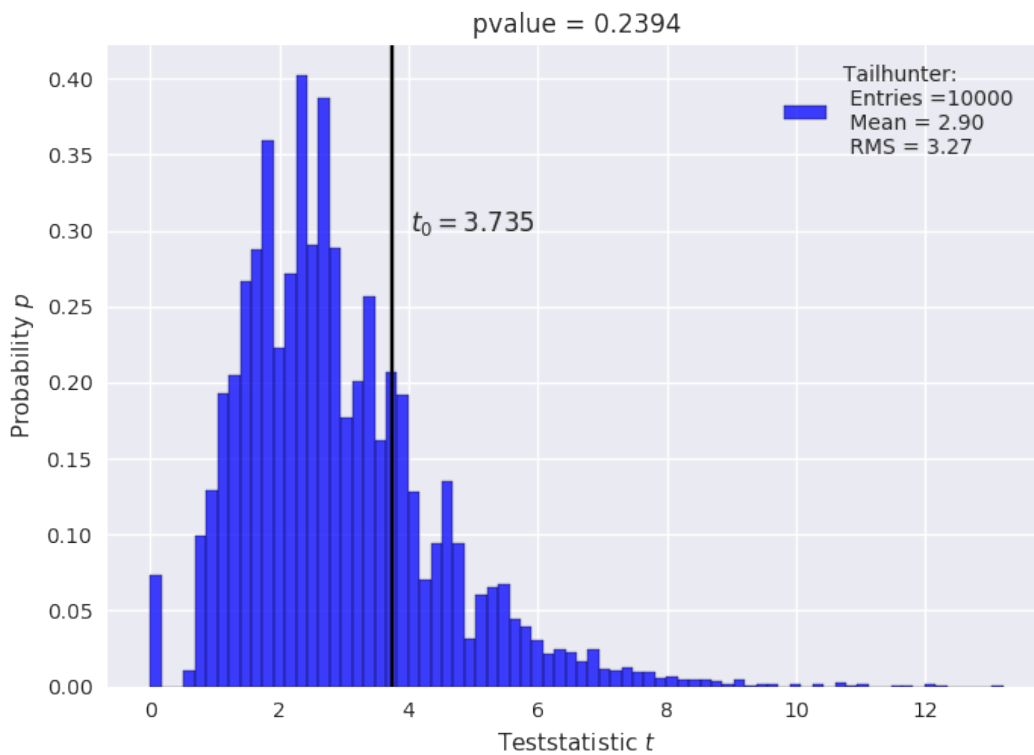


Figure 7.12: Distribution of the TailHunter test statistic with a p -value= 0.2394 after performing 10000 pseudo experiments.

7.4 Proof-of-Principle: Sanity Check

The results of Section 7.1 and Section 7.3 are compared with the official ATLAS results [65]. A sanity check is performed. The official ATLAS results are presented in Fig. 7.13 and the results of the Jupyter notebook are shown in Fig. 7.14.

Both figures show the data and the background prediction in the main panel. The official ATLAS figure has also included fits of the benchmark model which were not considered in this analysis. The middle panel shows the Poisson significance and the bottom panel the relative difference $(D - B)/B$. In the official ATLAS figure, the JES uncertainty is also shown in the bottom panel.

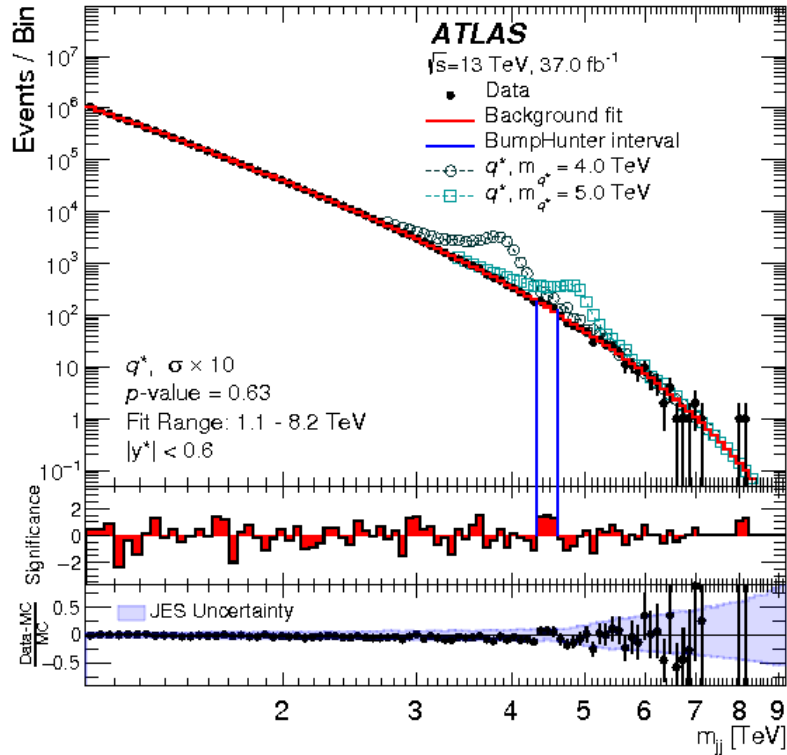


Figure 7.13: The official ATLAS figure [3] shows the significance, the relative difference, the BumpHunter interval and its p -value.

Exact values of the calculated relative difference and the significance are not published and therefore, a direct comparison between the official and the self-programmed results is not possible. Looking at both plots, the significance and the relative difference are very similar.

The BumpHunter results from Section 7.3.1 are

$$p\text{-value} \approx 0.6 - 0.7 \quad \text{and} \quad m_{jj} = 4.326 - 4.595 \text{ TeV}$$

The BumpHunter p -value is similar with $p\text{-value} = 0.63$ [3]. There differences come from the fact that the results of the pseudo experiments vary. The observed significant window is the same. That means, in both cases no significant excess in any window is observed and the results are in accordance.

The TailHunter was not performed in the official analysis [3]. Therefore, the results cannot be compared.

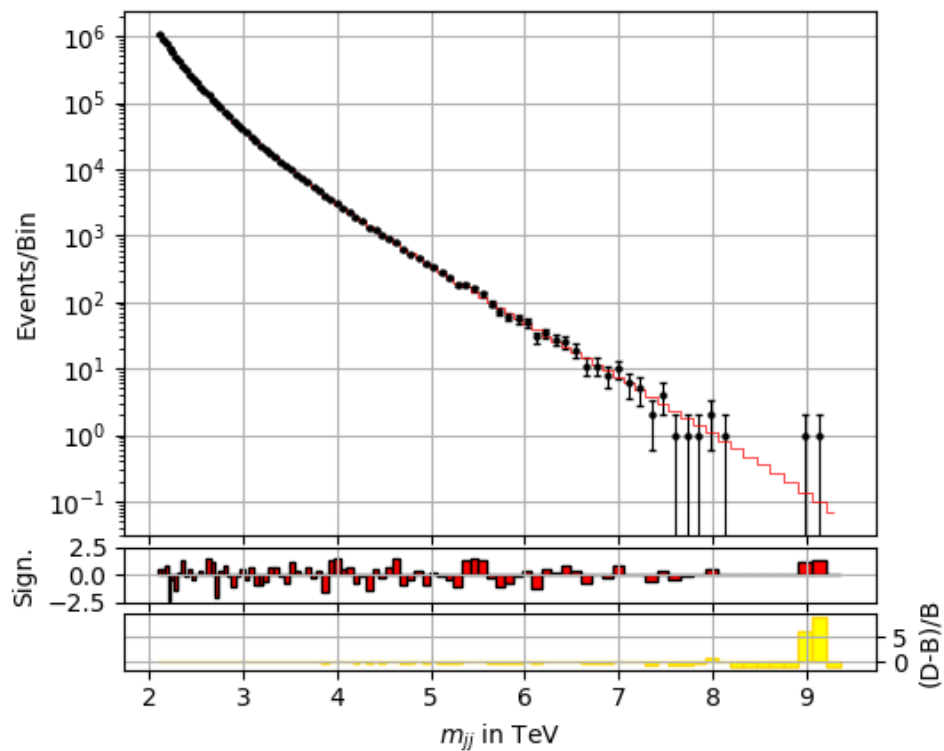


Figure 7.14: Results of the significance and the relative difference are shown in a subplot with data and background prediction.

8 Conclusion

A Jupyter notebook was designed describing the theory, experiment and the statistical analysis of the dijet search for new physics beyond the SM. This written elaboration of the notebook has been written to further detail the theory, experiment and methods. It guides the reader through the notebook and explains how it can be run.

The invariant mass m_{jj} of dijet events of a data set recorded in 2015 and 2016 with the ATLAS detector in proton-proton collisions at $\sqrt{s} = 13$ TeV corresponding to an integrated luminosity of 37 fb^{-1} were investigated. The Jupyter notebook comparing the data and the background prediction was validated by comparing the results with the results of the ATLAS collaboration. Consequently, no significant local excess between the measured data and the predicted background is observed. For dijet events with a rapidity difference of $|y^*| < 0.6$, the deviations of all the single bins lay below 2.4 standard deviations. Had it been three standard deviations, this would have been regarded as evidence.

The focus of the notebook is set on the statistical analysis of comparing a data set with a background prediction. Besides bin-by-bin analysis techniques, hypothesis hyper tests are introduced to get a global analysis of the spectrum.

In the first part of the analysis, different ways of bin-by-bin comparisons are applied and compared. It was shown that methods as depicting the absolute difference or the relative difference between data and background are not comparable with the significance. Additionally, it was shown that the Gaussian approximation of the significance for a Poisson distributed data set is only suitable for high-populated bins with at least 10 entries. As a consequence, the most reliable and exact way is to illustrate differences by the calculation of the significance via the p -value.

In the second part of the analysis, two global hypothesis tests were implemented: The BumpHunter and the TailHunter algorithm. The BumpHunter algorithm from Ref. [100] was adjusted and the feature of sidebands has been added. The BumpHunter algorithm investigates the differences between data and background prediction in a window by calculating the p -value for the set of bins in the window. Thereby, the most significant window was identified in the range of $4.326 - 4.596$ TeV. Using 10000 pseudo data sets created under the prediction of the background-only-hypothesis, a probability of around $p\text{-value} \approx 0.69$ to wrongly rule out the background was determined. The conversion of this p -value to a significance results in no significant deviation: 0 standard deviations. A sanity check with the official results has shown that the BumpHunter algorithm works properly and gets the same outcome of the bump range with a slightly higher p -value.

Then, the BumpHunter was adapted that it works as its TailHunter generalization. While in the ATLAS analysis, the search was focused on the excesses in form of bumps, this project also investigated the tail of the distribution. The TailHunter found the mass range of $m_{jj} = 7.904 - 8.364$ TeV as the tail with the largest deviation. The p -value has also been determined running 10000 sets of pseudo data following the background prediction. A $p\text{-value} = 0.2 - 0.3$ for the TailHunter gives a deviation of < 1 standard deviations which is not significant.

To conclude, a properly working program has been written analyzing differences between data and prediction progressively. The tool can be used in schools, workshops or other events for pupils and early students who may have developed an interest in particle physics data and statistical analysis.

A Statistics

A.1 Derivation of Poisson distribution

A.1.1 Approximation of Binomial to Poisson distribution

The binomial distribution

$$P(x|N, p) = \binom{N}{x} p^x (1-p)^{N-x}$$

with expectation value $\mu = N \cdot p = \text{const.}$ approximates the Poisson distribution for a large number of events N and $p \ll 1$.

The derivation is shown here:

$$\begin{aligned} P(x|N, p) &= \binom{N}{x} p^x (1-p)^{N-x} = \binom{N}{x} \left(\frac{\mu}{N}\right)^x \left(1 - \frac{\mu}{N}\right)^{N-x} \\ &= \frac{N!}{x!(N-x)!} \left(\frac{\mu}{N}\right)^x \left(1 - \frac{\mu}{N}\right)^{N-x} \\ &= \frac{N \cdot (N-1) \cdot \dots \cdot (N-x+1)}{x!} \frac{\mu^x}{N^x} \left(1 - \frac{\mu}{N}\right)^{N-x} \\ &= \frac{N}{N} \cdot \frac{N-1}{N} \cdot \dots \cdot \frac{N-x+1}{N} \cdot \frac{\mu^x}{x!} \cdot \left(1 - \frac{\mu}{N}\right)^N \cdot \left(1 - \frac{\mu}{N}\right)^{-x} \end{aligned}$$

For a large number of N , we get

$$\begin{aligned} \lim_{n \rightarrow \infty} P(x|N, p) &= \lim_{n \rightarrow \infty} \frac{N}{N} \cdot \frac{N-1}{N} \cdot \dots \cdot \frac{N-x+1}{N} \cdot \frac{\mu^x}{x!} \cdot \left(1 - \frac{\mu}{N}\right)^N \cdot \left(1 - \frac{\mu}{N}\right)^{-x} \\ &= \underbrace{\frac{N}{N}}_{=1} \cdot \underbrace{\frac{N-1}{N}}_{=1} \cdot \underbrace{\dots}_{=1} \cdot \underbrace{\frac{N-x+1}{N}}_{=1} \cdot \frac{\mu^x}{x!} \cdot \underbrace{\left(1 - \frac{\mu}{N}\right)^N}_{e^{-\mu}} \cdot \underbrace{\left(1 - \frac{\mu}{N}\right)^{-x}}_{=1} \\ &= \frac{\mu^x}{x!} \cdot e^{-\mu}. \end{aligned}$$

$$\Rightarrow P(x|\mu) = \frac{1}{x!} \mu^x e^{-\mu}$$

A.1.2 Derivation with Poisson assumptions

Another possibility is to derive the Poisson distribution directly [103]. It is g the probability for independent events in an infinitesimal small interval dl . The assumptions for a Poisson distribution are:

1. In the interval $[l, l + dl]$, the number of events is $x \leq 1$.
2. The probability for getting one event in $[l, l + dl]$ is $p = gdl$.
3. The event in an interval is independent from all other events.

With these assumptions, the probability to have one event in an interval with the length dl is

$$P_1 = gdl$$

and to have no event is given by

$$P_0 = 1 - gdl. \quad (\text{A.1})$$

Thus, the probability to have no event in an interval with the length $l + dl$ is calculated by the product

$$P_0(l + dl) = P_0(l) \cdot P_0(dl) \quad (\text{A.2})$$

which becomes with Eq. (A.1) to

$$\frac{P_0(l + dl) - P_0(l)}{dl} = -gP_0(l). \quad (\text{A.3})$$

The differential equation for an infinitesimal small $dl \rightarrow 0$

$$\frac{P_0(l)}{dl} = -gP_0(l)$$

has the solution

$$P_0(l) = e^{-gl}$$

for no event until l and $P_0(0) = 1$. The probability to get k events until $l + dl$ is calculated by

$$\begin{aligned} P_k(l + dl) &= P_k(l)P_0(dl) + P_{k-1}(l)P_1(dl) \\ &= P_k(l)(1 - gdl) + P_{k-1}(l)gdl \\ \Rightarrow \frac{P_k(l + dl) - P_k(l)}{dl} &= \frac{P_k(l)(1 - gdl) + P_{k-1}(l)gdl - P_k(l)}{dl} \\ &= P_{k-1}(l)g - P_k(l)g \\ &= -g(P_k(l) - P_{k-1}(l)) \end{aligned}$$

For an infinitesimal small dl , it becomes a differential equation

$$\frac{P_k(l)}{dl} = -g(P_k(l) - P_{k-1}(l))$$

with the solution

$$P_k(l) = \frac{1}{k!} (gl)^k e^{-gl}$$

This is the Poisson distribution with $\lambda = gl$.

A.2 Approximation of Poisson to Gaussian distribution

The limit of the Poisson distribution

$$P(x|\mu) = \frac{1}{x!} \mu^x e^{-\mu}$$

for large μ is the Normal distribution also called Gaussian distribution. The expectation value is $\mu = n \cdot p$. The counted events is roughly the expectation value $x = \mu(1 + \delta)$ with a small deviation $\delta \ll 1$ while $\mu \gg 1$. Using the Stirling formula [104]

$$x! \approx \sqrt{2\pi x} x^x e^{-x}$$

and replacing x , the Poisson distribution becomes

$$\begin{aligned} P(x|\mu) &= \frac{1}{x!} \mu^x e^{-\mu} = \frac{\mu^x e^{-\mu}}{\sqrt{2\pi x} x^x e^{-x}} \\ &= \frac{\mu^{\mu(1+\delta)} e^{-\mu} e^{\mu(1+\delta)}}{\sqrt{2\pi \mu(1+\delta)} (\mu(1+\delta))^{\mu(1+\delta)}} \\ &= \frac{e^{\mu\delta}}{\sqrt{2\pi \mu}} \frac{1}{(1+\delta)^{\mu(1+\delta)+\frac{1}{2}}}. \end{aligned}$$

For $\delta \ll 1$ and $\mu \gg 1$, $(1+\delta)^{\mu(1+\delta)+\frac{1}{2}}$ approximates to

$$\begin{aligned} (1+\delta)^{\mu(1+\delta)+\frac{1}{2}} &= \exp\left(\ln((1+\delta)^{\mu(1+\delta)+\frac{1}{2}})\right) = \exp\left(\ln(1+\delta) \cdot \left[\mu(1+\delta) + \frac{1}{2}\right]\right) \\ &\approx \exp\left(\left[\mu + \mu\delta + \frac{1}{2}\right] \cdot \left[\delta - \frac{\delta^2}{2} + \mathcal{O}(\delta^3)\right]\right) \\ &\approx \exp\left(\delta\mu + \frac{\delta}{2} + \delta^2 \frac{\mu}{2} - \frac{\delta^2}{4} + \mathcal{O}(\delta^3)\right) \\ &\approx \exp\left(\mu\delta + \delta^2 \frac{\lambda}{2} + \mathcal{O}(\delta^3)\right). \end{aligned}$$

by considering only the second order of δ .

$$\begin{aligned} \Rightarrow P(x|\mu) &= \frac{e^{\mu\delta}}{\sqrt{2\pi \mu}} \frac{1}{\exp\left(\mu\delta + \delta^2 \frac{\lambda}{2}\right)} = \frac{e^{-\mu\delta^2/2}}{\sqrt{2\pi \mu}} \\ &= \frac{1}{\sqrt{2\pi \mu}} e^{-\frac{(x-\mu)^2}{2\mu}} \end{aligned}$$

With $\mu = \sigma^2$ it becomes to the normal distribution

$$P(x|\mu, \sigma) = \frac{1}{\sqrt{2\pi \sigma^2}} \cdot e^{-\frac{(x-\mu)^2}{2\sigma^2}}.$$

Bibliography

- [1] “About CERN”. In: (Jan. 2012). URL: <http://cds.cern.ch/record/1997225>.
- [2] *Detector Technology*. accessed 9 Aug, 2018. URL: <http://atlas.cern/discover/detector>.
- [3] ATLAS Collaboration. “Search for new phenomena in dijet events using 37 fb^{-1} of pp collision data collected at $\sqrt{s} = 13 \text{ TeV}$ with the ATLAS detector”. In: *Phys. Rev. D* 96.5 (2017), p. 052004. DOI: 10.1103/PhysRevD.96.052004. arXiv: 1703.09127 [hep-ex].
- [4] (accessed 15 Jul, 2018). URL: http://jupyter-notebook-beginner-guide.readthedocs.io/en/latest/what_is_jupyter.html.
- [5] G. Choudalakis and D. Casadei. “Plotting the differences between data and expectation”. In: *The European Physical Journal Plus* 127.2 (Feb. 2012), p. 25. ISSN: 2190-5444. DOI: 10.1140/epjp/i2012-12025-y. URL: <https://doi.org/10.1140/epjp/i2012-12025-y>.
- [6] Georgios Choudalakis. “On hypothesis testing, trials factor, hypertests and the BumpHunter”. In: (2011). arXiv: 1101.0390.
- [7] Sheldon L. Glashow. “Partial-symmetries of weak interactions”. In: *Nuclear Physics* 22.4 (1961), pp. 579–588. ISSN: 0029-5582. DOI: [https://doi.org/10.1016/0029-5582\(61\)90469-2](https://doi.org/10.1016/0029-5582(61)90469-2). URL: <http://www.sciencedirect.com/science/article/pii/0029558261904692>.
- [8] Steven Weinberg. “A Model of Leptons”. In: *Phys. Rev. Lett.* 19 (21 Nov. 1967), pp. 1264–1266. DOI: 10.1103/PhysRevLett.19.1264. URL: <https://link.aps.org/doi/10.1103/PhysRevLett.19.1264>.
- [9] Abdus Salam. “Weak and Electromagnetic Interactions”. In: *Conf. Proc.* C680519 (1968), pp. 367–377.
- [10] Guy Coughlan and James Dodd. “Das Modell von Glashow-Weinberg-Salam”. In: *Elementarteilchen: Eine Einführung für Naturwissenschaftler*. Ed. by Hening Genz. Wiesbaden: Vieweg+Teubner Verlag, 1996, pp. 139–144. ISBN: 978-3-322-83120-0. DOI: 10.1007/978-3-322-83120-0_23. URL: https://doi.org/10.1007/978-3-322-83120-0_23.
- [11] M. Herrero. “The Standard Model”. In: *Techniques and Concepts of High Energy Physics X*. Ed. by T. Ferbel. Dordrecht: Springer Netherlands, 1999, pp. 1–59. ISBN: 978-94-011-4689-0. DOI: 10.1007/978-94-011-4689-0_1. URL: https://doi.org/10.1007/978-94-011-4689-0_1.
- [12] Leif Jönsson. “Lectures in Particle Physics”. In: (2017).
- [13] Brian R Martin and Graham Shaw. *Particle physics*. John Wiley & Sons, 2017.
- [14] Torbjorn Sjostrand. “Monte Carlo Generators”. In: *High-energy physics. Proceedings, European School, Aronsborg, Sweden, June 18-July 1, 2006*. 2006, pp. 51–74. arXiv: hep-ph/0611247 [hep-ph]. URL: <http://weblib.cern.ch/abstract?CERN-LCGAPP-2006-06>.
- [15] Robert M. Harris and Konstantinos Kousouris. “Searches for Dijet Resonances at Hadron Colliders”. In: *Int. J. Mod. Phys. A* 26 (2011), pp. 5005–5055. DOI: 10.1142/S0217751X11054905. arXiv: 1110.5302 [hep-ex].

- [16] Lydia Audrey Beresford. “Searches for dijet resonances using $s = 13$ TeV proton-proton collision data recorded by the ATLAS detector at the Large Hadron Collider”. PhD thesis. University of Oxford, 2017.
- [17] Katherine Freese. “Review of Observational Evidence for Dark Matter in the Universe and in upcoming searches for Dark Stars”. In: (2008). DOI: 10.1051/eas/0936016. eprint: arXiv:0812.4005.
- [18] Cristiano Alpigiani. “Searches for Dark Matter in ATLAS”. In: *5th Large Hadron Collider Physics Conference (LHCP 2017) Shanghai, China, May 15-20, 2017*. 2017. arXiv: 1708.09674 [hep-ex]. URL: <https://inspirehep.net/record/1620913/files/arXiv:1708.09674.pdf>.
- [19] O. Brüning, H. Burkhardt, and S. Myers. “The Standard Model and beyond”. In: *Progress in Particle and Nuclear Physics* 67.3 (2012), pp. 705–734. ISSN: 0146-6410. DOI: <https://doi.org/10.1016/j.ppnp.2012.03.001>. URL: <http://united-states.cern/physics/standard-model-and-beyond>.
- [20] S. Tomonaga. “On a Relativistically Invariant Formulation of the Quantum Theory of Wave Fields*[†]”. In: *Progress of Theoretical Physics* 1.2 (1946), pp. 27–42. DOI: 10.1143/PTP.1.27. eprint: /oup/backfile/content_public/journal/ptp/1/2/10.1143_ptp.1.27/2/1-2-27.pdf. URL: <http://dx.doi.org/10.1143/PTP.1.27>.
- [21] R. P. Feynman. “Relativistic cutoff for quantum electrodynamics”. In: *Phys. Rev.* 74 (1948), pp. 1430–1438. DOI: 10.1103/PhysRev.74.1430.
- [22] Julian Schwinger. “On Quantum-Electrodynamics and the Magnetic Moment of the Electron”. In: *Phys. Rev.* 73 (4 Feb. 1948), pp. 416–417. DOI: 10.1103/PhysRev.73.416. URL: <https://link.aps.org/doi/10.1103/PhysRev.73.416>.
- [23] David J Gross and Frank Wilczek. “Asymptotically free gauge theories. I”. In: *Physical Review D* 8.10 (1973), p. 3633.
- [24] H David Politzer. “Reliable perturbative results for strong interactions?” In: *Physical Review Letters* 30.26 (1973), p. 1346.
- [25] ATLAS Collaboration. “Observation of a new particle in the search for the Standard Model Higgs boson with the ATLAS detector at the LHC”. In: *Physics Letters B* 716.1 (2012), pp. 1–29. ISSN: 0370-2693. DOI: <https://doi.org/10.1016/j.physletb.2012.08.020>. URL: <http://www.sciencedirect.com/science/article/pii/S037026931200857X>.
- [26] F. Englert and R. Brout. “Broken Symmetry and the Mass of Gauge Vector Mesons”. In: *Phys. Rev. Lett.* 13 (9 Aug. 1964), pp. 321–323. DOI: 10.1103/PhysRevLett.13.321. URL: <https://link.aps.org/doi/10.1103/PhysRevLett.13.321>.
- [27] Peter W. Higgs. “Broken Symmetries and the Masses of Gauge Bosons”. In: *Phys. Rev. Lett.* 13 (16 Oct. 1964), pp. 508–509. DOI: 10.1103/PhysRevLett.13.508. URL: <https://link.aps.org/doi/10.1103/PhysRevLett.13.508>.
- [28] Ralf Rapp and Hendrik van Hees. “Heavy Quark Diffusion as a Probe of the Quark-Gluon Plasma”. In: (2008). arXiv: 0803.0901 [hep-ph].

- [29] K. G. Begeman, A. H. Broeils, and R. H. Sanders. “Extended rotation curves of spiral galaxies: dark haloes and modified dynamics”. In: *Monthly Notices of the Royal Astronomical Society* 249.3 (1991), pp. 523–537. DOI: 10.1093/mnras/249.3.523. eprint: /oup/backfile/content_public/journal/mnras/249/3/10.1093_mnras_249.3.523/2/mnras249-0523.pdf. URL: <http://dx.doi.org/10.1093/mnras/249.3.523>.
- [30] Vera C. Rubin and W. Kent Ford Jr. “Rotation of the Andromeda Nebula from a Spectroscopic Survey of Emission Regions”. In: *Astrophys. J.* 159 (1970), pp. 379–403. DOI: 10.1086/150317.
- [31] G. Altarelli, B. Mele, and M. Ruiz-Altaba. “Searching for new heavy vector bosons in $p\bar{p}$ colliders”. In: *Zeitschrift für Physik C Particles and Fields* 47.4 (Dec. 1990), pp. 676–676. ISSN: 1431-5858. DOI: 10.1007/BF01552335. URL: <https://doi.org/10.1007/BF01552335>.
- [32] Thomas G. Rizzo. “ Z' phenomenology and the LHC”. In: *Proceedings of Theoretical Advanced Study Institute in Elementary Particle Physics : Exploring New Frontiers Using Colliders and Neutrinos (TASI 2006): Boulder, Colorado, June 4-30, 2006*. 2006, pp. 537–575. arXiv: hep-ph/0610104 [hep-ph]. URL: <http://www-public.slac.stanford.edu/sciDoc/docMeta.aspx?slacPubNumber=slac-pub-12129>.
- [33] M. V. Chizhov and Gia Dvali. “Origin and Phenomenology of Weak-Doublet Spin-1 Bosons”. In: *Phys. Lett.* B703 (2011), pp. 593–598. DOI: 10.1016/j.physletb.2011.08.056. arXiv: 0908.0924 [hep-ph].
- [34] Yanyan Gao. *Searches for dijet resonances at high mass and other hadronic final states without MET with 13 TeV data*. Moriond/EW, La Thuille Italy. 2017.
- [35] U. Baur, M. Spira, and P. M. Zerwas. “Excited-quark and -lepton production at hadron colliders”. In: *Phys. Rev. D* 42 (3 Aug. 1990), pp. 815–824. DOI: 10.1103/PhysRevD.42.815. URL: <https://link.aps.org/doi/10.1103/PhysRevD.42.815>.
- [36] Victor A. Berezin. “Quantum black hole model and Hawking’s radiation”. In: *Phys. Rev.* D55 (1997), pp. 2139–2151. DOI: 10.1103/PhysRevD.55.2139. arXiv: gr-qc/9602020 [gr-qc].
- [37] Stephen Hawking. “Gravitationally Collapsed Objects of Very Low Mass”. In: *Monthly Notices of the Royal Astronomical Society* 152.1 (1971), pp. 75–78. DOI: 10.1093/mnras/152.1.75. eprint: /oup/backfile/content_public/journal/mnras/152/1/10.1093_mnras_152.1.75/3/mnras152-0075.pdf. URL: <http://dx.doi.org/10.1093/mnras/152.1.75>.
- [38] Caterina Doglioni. *Dijet searches in ATLAS at the LHC Run-2*. Oxford Seminar. 2015.
- [39] O. Brüning, H. Burkhardt, and S. Myers. “The Large Hadron Collider”. In: *Progress in Particle and Nuclear Physics* 67.3 (2012), pp. 705–734. ISSN: 0146-6410. DOI: <https://doi.org/10.1016/j.ppnp.2012.03.001>. URL: <http://www.sciencedirect.com/science/article/pii/S0146641012000695>.
- [40] ATLAS Collaboration. “The ATLAS Experiment at the CERN Large Hadron Collider”. In: *JINST* 3 (2008). Also published by CERN Geneva in 2010, S08003. 437 p. URL: <http://cds.cern.ch/record/1129811>.

- [41] ATLAS Collaboration. *ATLAS detector and physics performance: Technical Design Report, 1*. Technical Design Report ATLAS. Geneva: CERN, 1999. URL: <https://cds.cern.ch/record/391176>.
- [42] CERN. “Facts figures LHC Season 2”. In: (). eprint: https://press.cern/sites/press.web.cern.ch/files/file/backgrounder/2016/02/factsandfigures-en_0.pdf. URL: <https://press.cern/backgrounders/facts-figures>.
- [43] “Experiments”. In: (July 2012). URL: <http://cds.cern.ch/record/1997374>.
- [44] ATLAS Collaboraion. *ATLAS public twiki*. (accessed 17 Jul, 2018). URL: <https://twiki.cern.ch/twiki/bin/view/AtlasPublic/LuminosityPublicResultsRun2>.
- [45] Matthias Schott and Monica Dunford. “Review of single vector boson production in pp collisions at $\sqrt{s} = 7$ TeV”. In: *Eur. Phys. J. C* 74 (2014), p. 2916. DOI: 10.1140/epjc/s10052-014-2916-1. arXiv: 1405.1160 [hep-ex].
- [46] *ATLAS A giant detector at the Large Hadron Collider*. accessed 18 Jul, 2018. URL: <http://collider.physics.ox.ac.uk/img/layers.png>.
- [47] ATLAS Collaboration. “A Particle Consistent with the Higgs Boson Observed with the ATLAS Detector at the Large Hadron Collider”. In: *Science* 338.6114 (2012), pp. 1576–1582. ISSN: 0036-8075. DOI: 10.1126/science.1232005. eprint: <http://science.sciencemag.org/content/338/6114/1576.full.pdf>. URL: <http://science.sciencemag.org/content/338/6114/1576>.
- [48] *The Inner Detector*. accessed 9 Aug, 2018. URL: <http://atlas.cern/discover/detector/inner-detector>.
- [49] *Calorimeter*. accessed 9 Aug, 2018. URL: <http://atlas.cern/discover/detector/calorimeter>.
- [50] Venkatesh S Kaushik. “Electromagnetic Showers And Shower Detectors”. In: *Internal Documents, University of Texas at Arlington* (2002).
- [51] A. Ferrari and P. R. Sala. “Physics processes in hadronic showers”. In: *Frascati Phys. Ser.* 21 (2001). [31(2000)], pp. 31–55.
- [52] *Calorimeters Energy measurement*. (accessed on 10 Aug, 2018). URL: http://www.desy.de/~garutti/LECTURES/ParticleDetectorSS12/L10_Calorimetry.pdf.
- [53] Michael Hausschild. *Detectors - an introduction*. (accessed on 10 Aug, 2018). URL: <https://indico.cern.ch/event/572234/contributions/2449705/attachments/1415624/2167262/Detectors.pdf>.
- [54] M.Battaglieri. *EM calorimeters*. (accessed on 10 Aug, 2018). URL: <https://www.ge.infn.it/~batta/Lect3-hadrcal.pdf>.
- [55] ATLAS Collaboration. *Expected performance of the ATLAS experiment: detector, trigger and physics*. Geneva: CERN, 2009. URL: <http://cds.cern.ch/record/1125884>.
- [56] *Muon Spectrometer*. accessed 9 Aug, 2018. URL: <http://atlas.cern/discover/detector/muon-spectrometer>.
- [57] (accessed 15 Jul, 2018). URL: <https://jupyter.org/>.
- [58] (accessed 16 Jul, 2018). URL: <http://jupyter.org/install>.
- [59] (accessed 16 Jul, 2018). URL: <https://www.anaconda.com/distribution/>.

- [60] (accessed 16 Jul, 2018). URL: <https://pypi.org/project/pip/>.
- [61] (accessed 16 Jul, 2018). URL: <https://anaconda.org/conda-forge/jupyterlab>.
- [62] (accessed 16 Jul, 2018). URL: <https://mybinder.org/v2/gh/ipython/ipython-in-depth/master?filepath=binder/Index.ipynb>.
- [63] (accessed 16 Jul, 2018). URL: <https://hub.mybinder.org/user/ipython-ipython-in-depth-f0qrlajt/notebooks/binder/Index.ipynb>.
- [64] (accessed 16 Jul, 2018). URL: <https://swan.cern.ch>.
- [65] ATLAS Collaboration. “Jet energy scale measurements and their systematic uncertainties in proton-proton collisions at $\sqrt{s} = 13$ TeV with the ATLAS detector”. In: *Phys. Rev. D* 96.7 (2017), p. 072002. DOI: 10.1103/PhysRevD.96.072002. arXiv: 1703.09665 [hep-ex].
- [66] (accessed 15 Jul, 2018). URL: <https://root.cern.ch/python-and-root>.
- [67] (accessed 16 Jul, 2018). URL: https://nlesc.gitbooks.io/cern-root-conda-recipes/content/installing_root_via_anaconda.html.
- [68] Caterina Doglioni Attilio Andreazza. *(py)ROOT tutorial*. 2012. URL: <https://indico.cern.ch/event/184080/contributions/1455632/>.
- [69] (accessed 15 Jul, 2018). URL: <https://pandas.pydata.org/>.
- [70] (accessed 15 Jul, 2018). URL: <https://www.statsmodels.org/stable/index.html>.
- [71] (accessed 15 Jul, 2018). URL: <https://docs.scipy.org/doc/scipy/reference/stats.html>.
- [72] (accessed 15 Jul, 2018). URL: https://matplotlib.org/api/pyplot_api.html#module-matplotlib.pyplot.
- [73] *Table 1 of Search for new phenomena in dijet events using 37 fb^{-1} of pp collision data collected at $\sqrt{s} = 13$ TeV with the ATLAS detector*. Data Set. 2017. DOI: 10.17182/hepdata.77265.v2/t1.
- [74] ATLAS Collaboration. “Jet energy measurement with the ATLAS detector in proton-proton collisions at $\sqrt{s} = 7$ TeV”. In: *Eur. Phys. J. C* 73.3 (2013), p. 2304. DOI: 10.1140/epjc/s10052-013-2304-2. arXiv: 1112.6426 [hep-ex].
- [75] ATLAS Collaboration. “Jet energy measurement and its systematic uncertainty in proton-proton collisions at $\sqrt{s} = 7$ TeV with the ATLAS detector”. In: *Eur. Phys. J. C* 75 (2015), p. 17. DOI: 10.1140/epjc/s10052-014-3190-y. arXiv: 1406.0076 [hep-ex].
- [76] *Jet Calibration and Systematic Uncertainties for Jets Reconstructed in the ATLAS Detector at $\sqrt{s} = 13$ TeV*. Tech. rep. ATL-PHYS-PUB-2015-015. Geneva: CERN, July 2015. URL: <http://cds.cern.ch/record/2037613>.
- [77] *Jet global sequential corrections with the ATLAS detector in proton-proton collisions at $\sqrt{s} = 8$ TeV*. Tech. rep. ATLAS-CONF-2015-002. Geneva: CERN, Mar. 2015. URL: <https://cds.cern.ch/record/2001682>.
- [78] ATLAS Collaboration. “Performance of pile-up mitigation techniques for jets in pp collisions at $\sqrt{s} = 8$ TeV using the ATLAS detector”. In: *Eur. Phys. J. C* 76.11 (2016), p. 581. DOI: 10.1140/epjc/s10052-016-4395-z. arXiv: 1510.03823 [hep-ex].

- [79] Karishma Sekhon and Dante Amidei. “Search for New Particles Decaying to Hadronic Jets in Proton-Proton Collision at $\sqrt{s} = 13$ TeV”. Presented 04 May 2018. May 2018. URL: <http://cds.cern.ch/record/2319069>.
- [80] W Lampl et al. *Calorimeter Clustering Algorithms: Description and Performance*. Tech. rep. ATL-LARG-PUB-2008-002. ATL-COM-LARG-2008-003. Geneva: CERN, Apr. 2008. URL: <https://cds.cern.ch/record/1099735>.
- [81] Matteo Cacciari, Gavin P. Salam, and Gregory Soyez. “The Anti-k(t) jet clustering algorithm”. In: *JHEP* 04 (2008), p. 063. DOI: 10.1088/1126-6708/2008/04/063. arXiv: 0802.1189 [hep-ph].
- [82] Caterina Doglioni. “Measurement of the inclusive jet cross section with the ATLAS detector at the Large Hadron Collider”. PhD thesis. University of Oxford, 2011.
- [83] Matteo Cacciari and Gavin P. Salam. “Pileup subtraction using jet areas”. In: *Physics Letters B* 659.1 (2008), pp. 119–126. ISSN: 0370-2693. DOI: <https://doi.org/10.1016/j.physletb.2007.09.077>. URL: <http://www.sciencedirect.com/science/article/pii/S0370269307011094>.
- [84] Lucy Kogan. “Determining the Jet Energy Scale uncertainty in the ATLAS detector”. In: *Nuclear Instruments and Methods in Physics Research Section A: Accelerators, Spectrometers, Detectors and Associated Equipment* 718 (2013). Proceedings of the 12th Pisa Meeting on Advanced Detectors, pp. 86–87. ISSN: 0168-9002. DOI: <https://doi.org/10.1016/j.nima.2012.11.048>. URL: <http://www.sciencedirect.com/science/article/pii/S016890021201385X>.
- [85] Ariel Schwartzman. “Jet energy calibration at the LHC”. In: *Int. J. Mod. Phys. A* 30.31 (2015), p. 1546002. DOI: 10.1142/S0217751X15460021. arXiv: 1509.05459 [hep-ex].
- [86] *TeV-scale jet energy calibration using multijet events including close-by jet effects at the ATLAS experiment*. Tech. rep. ATLAS-CONF-2013-003. Geneva: CERN, Jan. 2013. URL: <http://cds.cern.ch/record/1504740>.
- [87] ATLAS Collaboration. “A measurement of the calorimeter response to single hadrons and determination of the jet energy scale uncertainty using LHC Run-1 *pp*-collision data with the ATLAS detector”. In: *Eur. Phys. J. C* 77.1 (2017), p. 26. DOI: 10.1140/epjc/s10052-016-4580-0. arXiv: 1607.08842 [hep-ex].
- [88] *Selection of jets produced in 13TeV proton-proton collisions with the ATLAS detector*. Tech. rep. ATLAS-CONF-2015-029. Geneva: CERN, July 2015. URL: <https://cds.cern.ch/record/2037702>.
- [89] *Comparison of jet trigger in 2015 and 2016*. Tech. rep. ATL-COM-DAQ-2016-087. Geneva: CERN, July 2016. URL: <https://cds.cern.ch/record/2200390>.
- [90] CDF Collaboration. “Search for new particles decaying into dijets in proton-antiproton collisions at $s^{*1/2} = 1.96$ -TeV”. In: *Phys. Rev. D* 79 (2009), p. 112002. DOI: 10.1103/PhysRevD.79.112002. arXiv: 0812.4036 [hep-ex].
- [91] ATLAS Collaboration. “Search for New Particles in Two-Jet Final States in 7 TeV Proton-Proton Collisions with the ATLAS Detector at the LHC”. In: *Phys. Rev. Lett.* 105 (2010), p. 161801. DOI: 10.1103/PhysRevLett.105.161801. arXiv: 1008.2461 [hep-ex].

- [92] CMS Collaboration. “Search for Dijet Resonances in 7 TeV pp Collisions at CMS”. In: *Phys. Rev. Lett.* 105 (21 Nov. 2010), p. 211801. DOI: 10.1103/PhysRevLett.105.211801. URL: <https://link.aps.org/doi/10.1103/PhysRevLett.105.211801>.
- [93] ATLAS Collaboration. “Search for New Physics in Dijet Mass and Angular Distributions in pp Collisions at $\sqrt{s} = 7$ TeV Measured with the ATLAS Detector”. In: *New J. Phys.* 13 (2011), p. 053044. DOI: 10.1088/1367-2630/13/5/053044. arXiv: 1103.3864 [hep-ex].
- [94] CMS Collaboration. “Search for Resonances in the Dijet Mass Spectrum from 7 TeV pp Collisions at CMS”. In: *Phys. Lett.* B704 (2011), pp. 123–142. DOI: 10.1016/j.physletb.2011.09.015. arXiv: 1107.4771 [hep-ex].
- [95] ATLAS Collaboration. “Search for new phenomena in the dijet mass distribution using $p-p$ collision data at $\sqrt{s} = 8$ TeV with the ATLAS detector”. In: *Phys. Rev.* D91.5 (2015), p. 052007. DOI: 10.1103/PhysRevD.91.052007. arXiv: 1407.1376 [hep-ex].
- [96] ATLAS Collaboration. “Search for resonances in the mass distribution of jet pairs with one or two jets identified as b -jets in proton–proton collisions at $\sqrt{s} = 13$ TeV with the ATLAS detector”. In: *Phys. Lett.* B759 (2016), pp. 229–246. DOI: 10.1016/j.physletb.2016.05.064. arXiv: 1603.08791 [hep-ex].
- [97] *Search for resonances below 1.2 TeV from the mass distribution of b -jet pairs in proton-proton collisions at $\sqrt{s}=13$ TeV with the ATLAS detector*. Tech. rep. ATLAS-CONF-2016-031. Geneva: CERN, June 2016. URL: <https://cds.cern.ch/record/2161136>.
- [98] *Search for new phenomena in dijet events using 37 fb^{-1} of pp collision data collected at $\sqrt{s} = 13$ TeV with the ATLAS detector*. Data Collection. 2017. DOI: 10.17182/hepdata.77265.v2.
- [99] Roger J Barlow. *Statistics: a guide to the use of statistical methods in the physical sciences*. Vol. 29. John Wiley & Sons, 1989.
- [100] Peter Waller. *Simple implementation of the BumpHunter algorithm*. <https://github.com/pwaller/bumphunter.pw>. 2013.
- [101] Eilam Gross and Ofer Vitells. “Trial factors for the look elsewhere effect in high energy physics”. In: (2010). DOI: 10.1140/epjc/s10052-010-1470-8. eprint: arXiv:1005.1891.
- [102] Eilam Gross and Ofer Vitells. “Trial factors for the look elsewhere effect in high energy physics”. In: *The European Physical Journal C* 70.1 (Nov. 2010), pp. 525–530. ISSN: 1434-6052. DOI: 10.1140/epjc/s10052-010-1470-8. URL: <https://doi.org/10.1140/epjc/s10052-010-1470-8>.
- [103] Markus Schumacher. *private communiaction*.
- [104] Persi Diaconis and David Freedman. “An elementary proof of Stirling’s formula”. In: *The American Mathematical Monthly* 93.2 (1986), pp. 123–125.

Acknowledgements

Here, I would like to say thank you to all people who have supported me with this thesis. A few people I would like to highlight:

Markus Schumacher, my supervisor in Freiburg - thank you for taking over the supervision of my thesis and the topic, giving me new inputs and the interesting talks about physics and co.

Caterina Doglioni, my supervisor in Lund - thank you for providing such an interesting topic and the pleasant working atmosphere, for giving me the feeling that my project is useful and can have a future.

Kathrin Becker, my advisor - thank you for all the thought-provoking impulses, advises and comments on my thesis.

Wiliam Kalderon - thank you for the troubleshooting with the notebook and all the interesting inputs.

My colleges in Lund and Freiburg - thank you for the good working atmosphere, the encouraging and deflective conversations, the funny fika and lunche times.

Dennis and Alexandra - thank you for reading my drafts, giving comments and encouraging me all the time.

And last but not least: My family and friends, especially Mama, Papa, Michi und Wiebke - thank you for supporting and helping me in any situation which includes organizing all the stuff when I was already in Uppsala.

